WAPD-TM-1421
DOE RESEARCH AND
DEVELOPMENT REPORT

NUCLEAR ANALYSIS AND PERFORMANCE OF THE LIGHT WATER BREEDER REACTOR (LWBR) CORE POWER OPERATION AT SHIPPINGPORT

(LWBR Development Program)

APRIL 1984

CONTRACT DE-AC11-76PN00014

BETTIS ATOMIC POWER LABORATORY
WEST MIFFLIN, PENNSYLVANIA 15122-0079
Operated for the U.S. Department of Energy
WESTINGHOUSE ELECTRIC CORPORATION

87718CVR

DISCLAIMER

UC-78: Light Water Reactor Techology
DOE/TIC-4500 (REV. 73)

NUCLEAR ANALYSIS AND PERFORMANCE OF THE LIGHT WATER BREEDER REACTOR (LWBR) CORE POWER OPERATION AT SHIPPINGPORT

(LWBR Development Program)

H. C. Hecker

April 1984

WAPD-TM--1421

DE84 011834

Contract No. DE-AC11-76PN00014

Printed in the United States of America
Available from the
National Technical Information Service
U. S. Department of Commerce
5285 Port Royal Road
Springfield, Virginia 22151

NOTE

This document is an interim memorandum prepared primarily for internal reference and does not represent a final expression of the opinion of Westinghouse. When this memorandum is distributed externally, it is with the express understanding that Westinghouse makes no representation as to completeness, accuracy or usability of information contained therein.

BETTIS ATOMIC POWER LABORATORY WEST MIFFLIN, PENNSYLVANIA

Operated for the U.S. Department of Energy
by
WESTINGHOUSE ELECTRIC CORPORATION

MASTER

DISCLAIMER

NOTICE

FOREWORD

The Shippingport Atomic Power Station located in Shippingport, Pennsylvania was the first large-scale, central-station nuclear power plant in the United States and the first plant of such size in the world operated solely to produce electric power. This program was started in 1953 to confirm the practical application of nuclear power for large-scale electric power generation. It has provided much of the technology being used for design and operation of the commercial, central-station nuclear power plants now in use.

Subsequent to development and successful operation of the Pressurized Water Reactor in the Atomic Energy Commission (now Department of Energy, DOE) owned reactor plant at the Shippingport Atomic Power Station, the Atomic Energy Commission in 1965 undertook a research and development program to design and build a Light Water Breeder core for operation in the Shippingport Station.

The objective of the Light Water Breeder Reactor (LWBR) program has been to develop a technology that would significantly improve the utilization of the nation's nuclear fuel resources employing the well-established water reactor technology. To achieve this objective, work has been directed toward analysis, design, component tests, and fabrication of a water-cooled, thorium oxide-uranium oxide fuel cycle breeder reactor for installation and operation at the Shippingport Station. The LWBR core started operation in the Shippingport Station in the Fall of 1977 and finished routine power operation on October 1, 1982. The End-of-Life test program has been completed. The core is being removed and the spent fuel shipped to the Naval Reactors Expended Core Facility for detailed examination to verify core performance including an evaluation of breeding characteristics.

In 1976, with fabrication of the Shippingport LWBR core nearing completion, the Energy Research and Development Administration, now DOE, established the Advanced Water Breeder Applications (AWBA) program to develop and disseminate technical information which would assist U.S. industry in evaluating the LWBR concept for commercial-scale applications. The AWBA program, which was concluded in September, 1982, explored some of the problems that would have been faced by industry in adopting technology confirmed in the LWBR program. Information developed includes concepts for commercial-scale prebreeder cores which would produce uranium-233 for light water breeder cores while producing electric power, improvements for breeder cores based on the technology developed to fabricate and operate the Shippingport LWBR core, and other information and technology to aid in evaluating commercial-scale application of the LWBR concept.

All three development programs (Pressurized Water Reactor, Light Water Breeder Reactor, and Advanced Water Breeder Applications) have been conducted under the technical direction of the Office of the Duputy Assistant Secretary for Naval Reactors of DOE.

Technical information developed under the Shippingport, LWBR, and AWBA programs has been and will continue to be published in technical memoranda, one of which is this present report.

INTENTIONALLY BLANK

TABLE OF CONTENTS

NUCLEAR ANALYSIS AND PERFORMANCE OF THE LIGHT WATER BREEDER REACTOR (LWBR) CORE POWER OPERATION AT SHIPPINGPORT

(LWBR Development Program)

H. C. Hecker

April 1984

This report presents the nuclear analysis and discusses the performance of the LWBR core at Shippingport during power operation from initial startup through end-of-life at 28,730 EFPH. Core follow depletion calculations confirmed that the reactivity bias and power distributions were well within the uncertainty allowances used in the design and safety analysis of LWBR. The magnitude of the core follow reactivity bias has shown that the calculational models used can predict the behavior of U^{233}-Th systems with closely spaced fuel rod lattices and movable fuel. In addition, the calculated final fissile loading is sufficiently greater than the initial fissile inventory that the measurements to be performed for proof-of-breeding evaluations are expected to confirm that breeding has occurred.

WAPD-TM-1421

NUCLEAR ANALYSIS AND PERFORMANCE OF THE LIGHT WATER BREEDER REACTOR (LWBR) CORE POWER OPERATION AT SHIPPINGPORT

(LWBR Development Program)

H. C. Hecker

I. INTRODUCTION AND SUMMARY

Light Water Breeder Reactor (LWBR) core operation at the Shippingport Atomic Power Station provided electricity to the Duquesne Light Company system from September 1977 to October 1, 1982 and generated 2.1 billion kilowatt hours electric gross and 1.7 billion kilowatt hours electric net. This report presents a summary of the LWBR operation and nuclear analyses of core performance during power operation. A series of periodic tests was performed during core operation to confirm the adequacy of the LWBR nuclear design and to qualify the calculational model used in the analysis of the LWBR nuclear performance. Results of the LWBR physics test program are presented in References 1, 2 and 3.

LWBR achieved 28,730 effective full power hours (EFPH) during 5 years without refueling, which is equivalent to an average of about 14,600 MWd/t depletion. Peak local depletion was about 54,000 MWd/t in the seed region and 25,000 MWd/t in the blanket region. Operation during the first three years included nominal full power operation at 236.6 MW(th) (about 60 MWe net electrical), four planned semi-annual shutdowns for training, maintenance and testing, and 204 planned load following cycles (swingloads). During swingload cycles, power was reduced to between 60 and 35 percent for periods of from four to eight hours. Swingload cycles were performed as a demonstration of fuel element and plant capability to follow load demand for a typical utility power

system. Based on periodic radiochemical sampling of the coolant, there has been no indication of fuel element failure. These operations during the first three years achieved 18,298 EFPH (≃ 9300 MWd/t average depletion), exceeding the design lifetime of 18,000 EFPH.

During the last two years, maximum power level operation was primarily at 80 percent of nominal full power, with four planned shutdowns for testing, including the final October 1, 1982 shutdown. To reduce the duty requirements on the fuel elements during this period of extended lifetime, and to lengthen the reactivity lifetime of the core, reductions were made in operating temperature and pressure, as well as maximum power after 18,298 EFPH had been achieved. The end of reactivity lifetime at a maximum power level of 80% was reached at about 27,100 EFPH with the 12 movable seed assemblies* at the maximum withdrawn position. A further extension in lifetime of about 6% was obtained by a gradual power coastdown to 57% power prior to the final shutdown at 28,730 EFPH. The overall capacity factor was about 65% in spite of the extensive test periods and the reduced power operation.

Nuclear performance of the LWBR core was monitored approximately monthly throughout core life through determination of the reactivity bias of the core. Bias results show that the core was more reactive than calculated at full power and that the reactivity difference between prediction and calculation, bias, increased during lifetime. Reactivity bias during power operation ranged from a minimum of 0.15 percent overreactive near beginning-of-life to a maximum of 0.54 percent overreactive late in core life.

---

*In LWBR, the control elements are movable fuel (movable seed) assemblies. See Section II.

Breeding parameters for the LWBR were also evaluated throughout core life. Fuel depletion calculations which approximated the actual power operations indicate that more fissile fuel was produced in the core than was consumed. The calculated final fissile fuel content is 1.3 percent greater than the initial fissile fuel inventory.

Sections II and III of this report provide a brief description of the LWBR core and the methods used for performing the nuclear analysis of core performance during power operation.

Details of the LWBR core performance presented in Section IV include data on the power operating history, reactivity bias evaluations, breeding and fuel distribution, and power distribution and power performance. Section V presents a more detailed discussion of conclusions and a summary of how the LWBR nuclear design and performance objectives were met.

II. DESCRIPTION OF THE CORE AND FUEL SYSTEM

The light water breeder reactor (LWBR) core is a pressurized, light water moderated and cooled, thermal breeder which was designed for installation in the existing reactor vessel at the Shippingport Atomic Power Station (SAPS). At full rated power the LWBR core produced 236.6 thermal megawatts (MWt) which was converted to about 72 gross electrical megawatts (MWe). The core was operated at an average primary coolant temperature of 531°F from beginning-of-life to 18,298 EFPH and at 521 ± 3°F from 18,298 EFPH to end-of-life (28,730 EFPH). The pressure at beginning-of-life was 1985 pounds per square inch, gauge (psig) and was reduced to 1925 psig at 4,254 EFPH, 1855 psig at 7,028 EFPH, 1800 psig at

10,771 EFPH, and to 1585 psig from 18,298 EFPH to end-of-life. The temperature and pressure changes were made to reduce duty requirements on core and plant components.

The LWBR core was designed to breed using the uranium-233/thorium fuel cycle in a pressurized light water reactor plant. Reasons why breeding can be achieved in a light water reactor using the uranium-233/thorium fuel system and design features implemented in the LWBR core to enhance fuel utilization were presented in Reference 4. In essence, sufficient neutrons are produced per neutron absorbed (η) for U^{233} to sustain breeding in an appropriate light water reactor design. U^{233} is the only fissile isotope capable of thermal breeding in a practicable system. The core was designed to minimize parasitic neutron losses in core and structural materials, and reactivity was controlled with minimum parasitic neutron loss using movable fuel control (i.e., variable geometry control). This reactor is the only uranium-233/thorium power reactor ever to be operated, making the performance results unique as well as important to demonstrating high fuel utilization technology.

A. Fuel Modules and Fuel Assemblies

Figure II-1 presents a cross-sectional view of the LWBR core showing the orientation and types of modules which comprise the core configuration. As shown, the core contained the following types of fuel modules and fuel assemblies:

1. Twelve identical hexagonal movable seed assemblies.

2. Twelve stationary annular hexagonal blanket fuel assemblies, which combined with movable seed assemblies to form seed-and-blanket modules. Of the 12 stationary blanket fuel assemblies, nine were composed of two blanket regions denoted as standard blanket and power-flattening blanket regions, as shown on Figure II-1.
3. Fifteen reflector blanket fuel modules.

The seed-and-blanket modules contained both fissile uranium-233 and fertile thorium-232, in the form of pellets of $U^{233}O_2$-ThO_2 in Zircaloy-clad fuel rods. Seed assemblies contained relatively high fissile weight percents (4.3 and 5.2) and the blanket assemblies had somewhat lower fissile weight percents (1.2 to 2.7). The reflector blanket fuel modules initially contained only thorium in the form of ThO_2 pellets in Zircaloy-clad fuel rods.

The three central seed-and-blanket modules (Type I modules), shown in Figure II-2, were designed to be typical of those which could be utilized in a large light water breeder reactor plant. The surrounding nine seed-and-blanket modules (Type II and III modules) had a larger outer (power-flattening) blanket region that was fueled with a higher uranium-233 content and had a larger water volume fraction than the inner blanket region. This outer blanket region was nuclearly more reactive than the inner blanket region and produced a more uniform power distribution within the interior of the core, thereby better simulating the breeding environment of a typical large core. This arrangement was required due to the constraint imposed by use of the relatively small Shippingport pressure vessel. The 15 reflector blanket fuel modules surrounded the interior 12 seed-and-blanket modules and served to reduce neutron leakage from the relatively small Shippingport core. Surrounding the reflector blanket

fuel modules were 15 stainless steel, non-fuel filler units whose purpose was to limit flow leakage by filling the space between the reflector modules and the core barrel. The entire core was assembled inside the 109 inch inner diameter Shippingport reactor vessel. A more comprehensive description of the LWBR core is given in Reference 5.

B. Reactivity Control and Fuel Distribution

To eliminate the parasitic loss of neutrons in conventional control poison materials and thereby to enhance breeding in a light water, uranium-233/thorium environment, LWBR core reactivity control was achieved entirely by varying the geometric relationship between the movable seed assemblies and the associated stationary annular blanket assemblies which surrounded each seed assembly. For LWBR operation, this reactivity control was achieved by uniformly positioning the 12 movable seed assemblies in a bank by means of individual control drive mechanisms. Each movable seed assembly was positioned axially within its associated annular blanket assembly to achieve core reactivity control. This unique control method was analogous in operation to that of conventional poison rod control in that negative reactivity addition and core shutdown were achieved by lowering the control elements and positive reactivity addition was achieved by raising the control elements.

Figure II-3 shows an axial elevation sketch of a seed-and-blanket module. At the shutdown position with all movable seed assemblies disengaged from the control drive mechanisms, the bottoms of the movable seed assemblies were 60 inches below the bottoms of the blanket assemblies. To achieve criti-

cality and bring the core to power, the movable seed assemblies were lifted so that they were more nearly in axial alignment with the blanket fuel assemblies. The maximum withdrawn position was 24 inches above the aligned position. Thus the full length of travel of the seed modules was 84 inches.

All rods had a nominal fuel pellet stack height of 104 inches. The maximum length of the binary segment, $U^{233}O_2$ - ThO_2, in a fuel rod was 84 inches. There were ThO_2 reflector segments of about 10 inches on each end of the rods. Rods adjacent to the seed-blanket interfaces had longer ThO_2 segments and shorter binary segments to enhance reactivity control. These ThO_2 segments which are in the upper portion of the seed assembly and the lower portion of the blanket assembly were designed to give a ThO_2 step region on both sides of the seed-blanket interface. With this arrangement, lowering the movable seed assemblies increased the thoria thickness separating the seed and blanket binary fuel and resulted in lower reactivity. The fuel worth ($\Delta\rho$/inch) achieved by this fuel distribution was largest for low positions of the movable fuel and smallest for high positions of the movable fuel. As the core depleted, U-233 was produced in the thoria step regions, reducing movable fuel worth.

Selection of the initial uranium-233 loading distribution between seed and blanket included other considerations. Reactivity was balanced between seed and blanket to yield adequate lifetime with a critical movable fuel position at beginning-of-life not too far below the aligned position. This was desirable since the neutron losses increase with seed-blanket axial fuel displacement from the aligned position (Figure II-3). At the same time, the movable fuel

reactivity worth as a function of position was designed to provide adequate shutdown capability. Specification of uranium-233 loading variation in radial zones within seed and blanket assemblies was also designed to reduce power peaking in the vicinity of metal/water channels.

The total initial fissile loading (U-233 plus U-235) of the LWBR core was approximately 501 kilograms. Initial loading and calculated final fissile loading data for each module are presented in the discussion of breeding performance (Section IV.C). Additional details on the fuel system and initial core loading distribution are given in Reference 6. Also, a summary of as-built data for fuel rods, support grids, and modules in the LWBR core is presented in Appendix A of Reference 6.

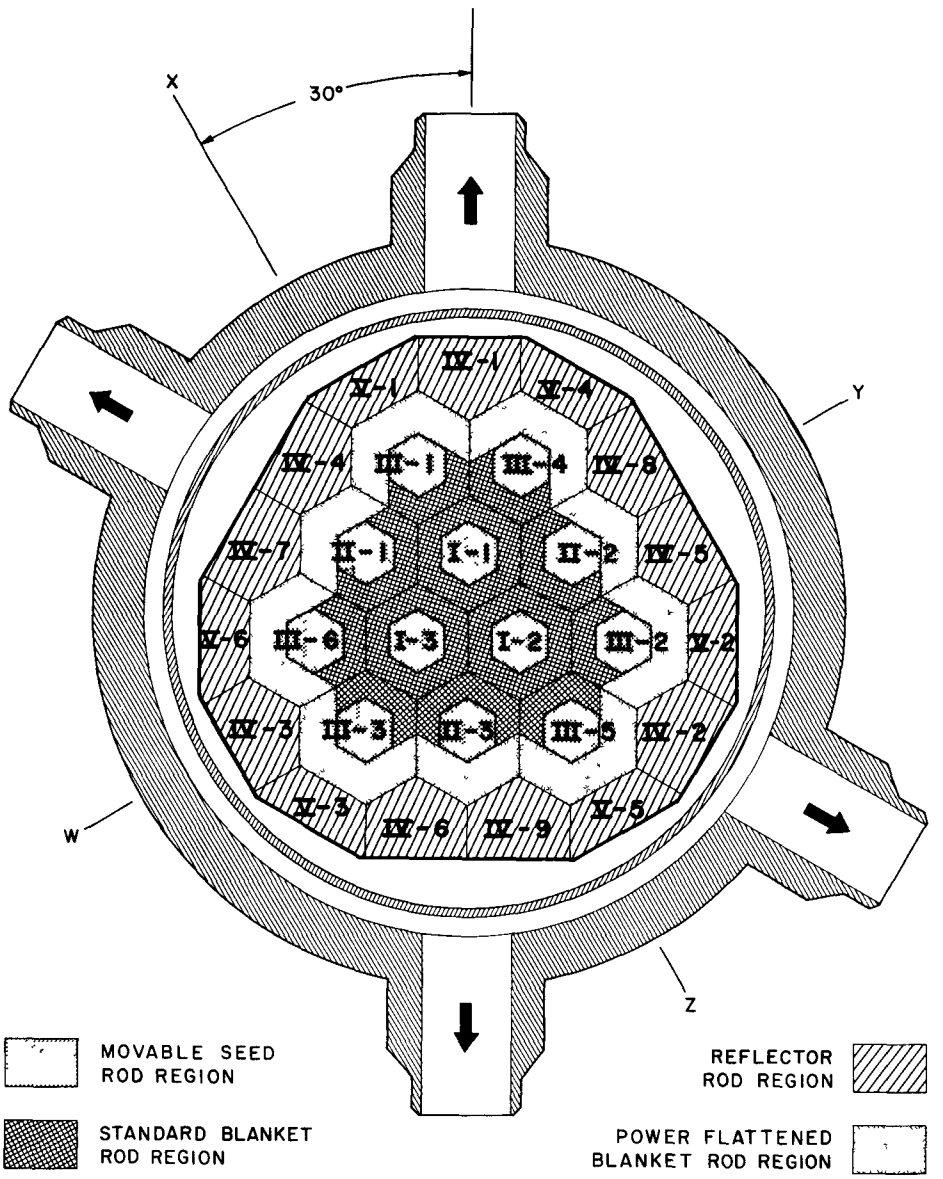

FIGURE II-1 LWBR CROSS SECTION MODULE IDENTIFICATION

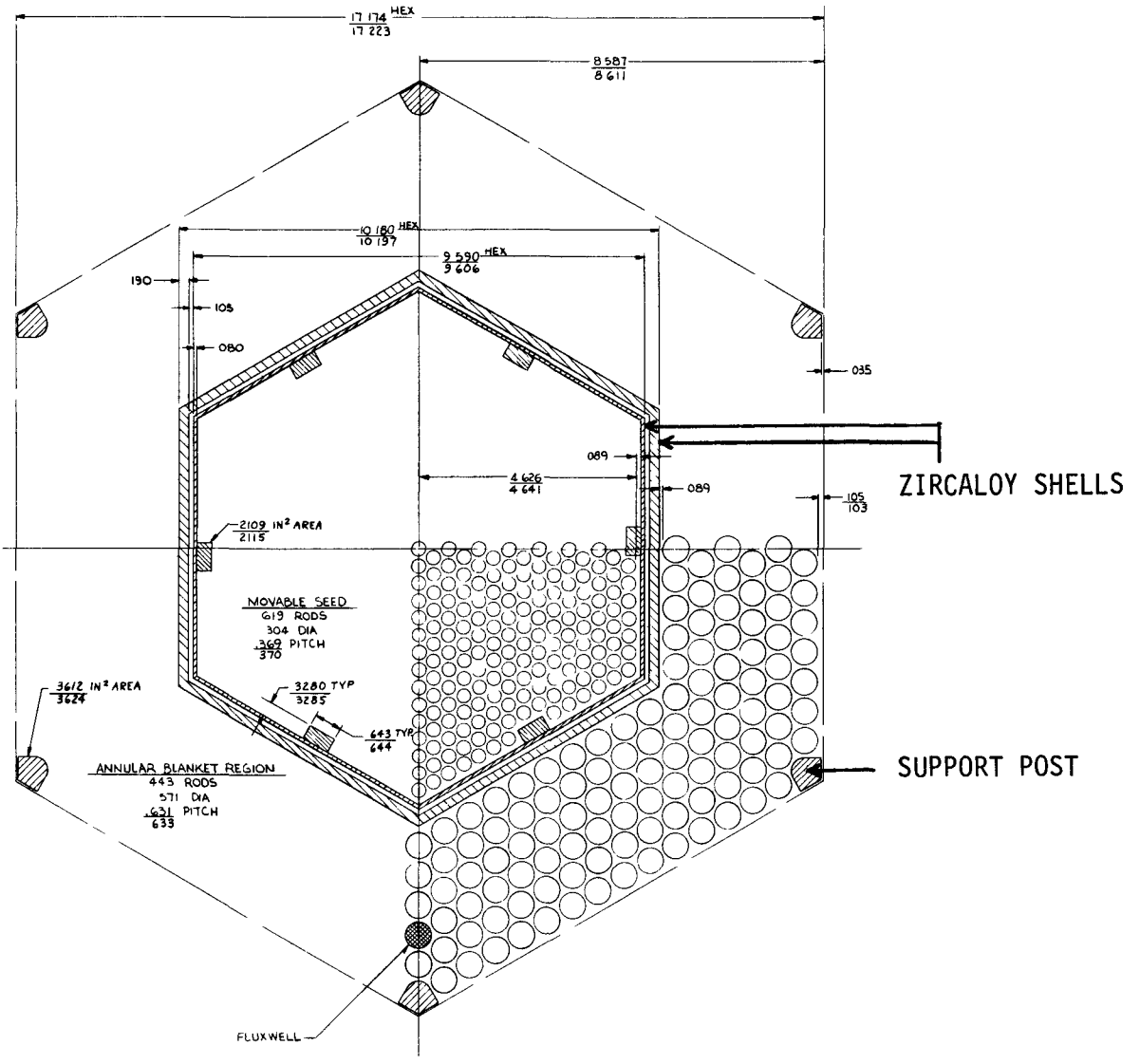

FIGURE II-2 TYPE I MODULE CROSS SECTION

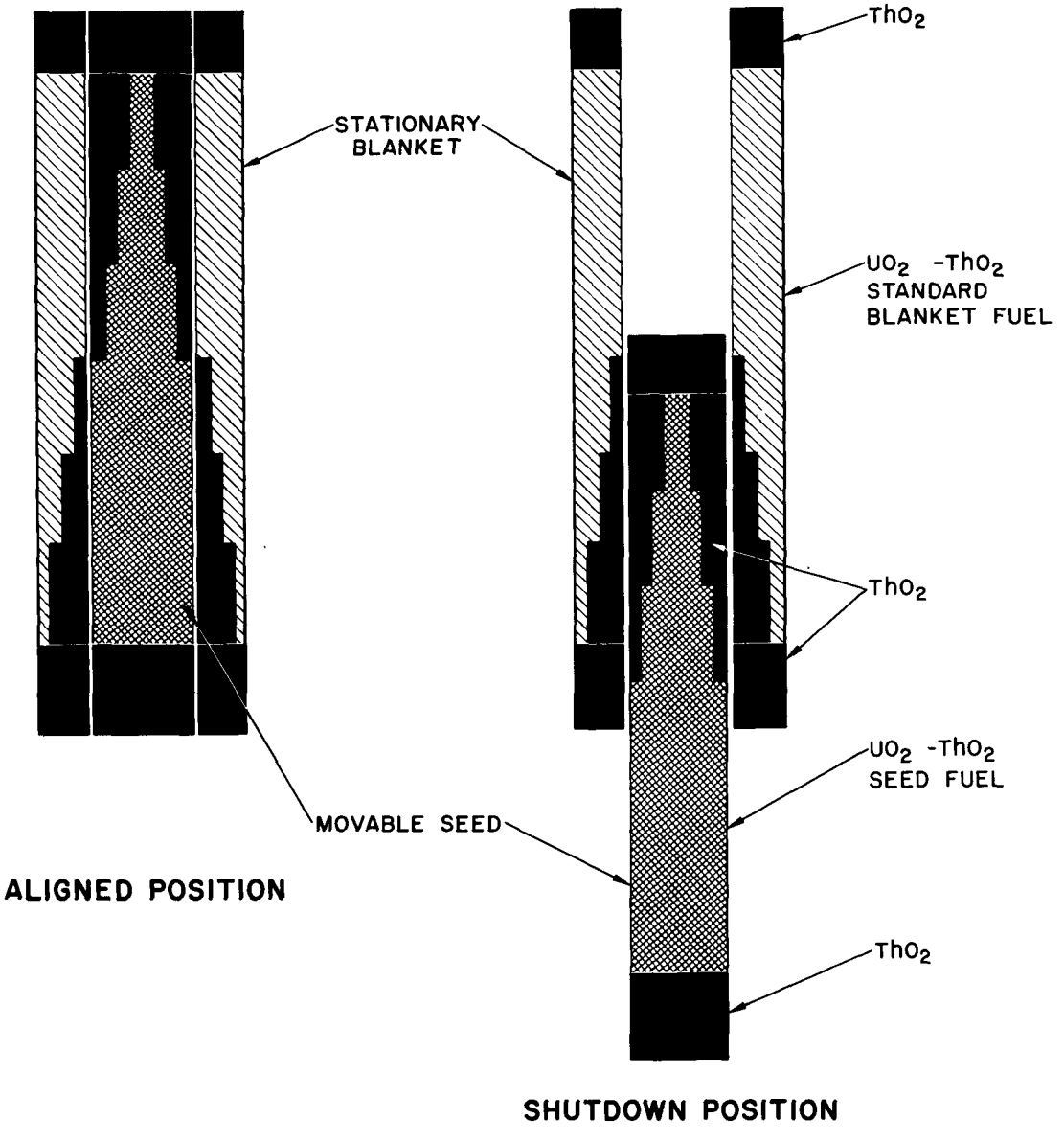

FIGURE II-3 MOVABLE FUEL CONTROL

III. BASIS FOR LWBR NUCLEAR PERFORMANCE EVALUATION

The calculational model used in the analysis of the nuclear performance of the LWBR core was qualified with the aid of many comparisons of calculations to experiments and with comparisons to calculational standards. This extensive qualification program provided confidence in the fundamental data developed for U-233 and Th-232 and has verified the ability to calculate the nuclear characteristics of the LWBR core. A detailed description of the calculational model and its qualification is presented in Reference 7. This section, therefore, will present a brief summary of the analysis methods.

Performance characteristics for the LWBR core were calculated using four group diffusion theory in two- and three-dimensional PDQ (Reference 8) calculations, with few-group constants obtained from the energy spectrum program PAX (References 7, 9 and 10). Two-dimensional R-Z calculations were performed for a central (Type I) module, and three-dimensional calculations were performed for either a symmetric one-sixth or one-half of the core, depending upon the symmetry of the case being analyzed. Most calculations were performed with a three-dimensional one-sixth core geometry to represent the full core since LWBR had sixth core symmetry (see Figure II-1) under normal operating conditions. The R-Z calculations were used to obtain reactivity bias corrections for short depletion intervals relative to the longer depletion intervals used in the one-sixth core calculations. Half core calculations were done for various physics test configurations where movable seed assemblies were not in a uniform level bank position.

Features of the calculational model, described in detail in Reference 7, included:

1. An automated system of processing manufacturing data for direct input to the PAX and PDQ nuclear analysis programs;
2. Extensive evaluation and qualification of nuclear data for the Th-U^{233} fuel system;
3. Accurate deterministic heterogeneous resonance integral calculations which account for self-shielding and mutual-shielding without the need for correction factors;
4. Accounting for neutron energy spectrum changes in fuel zones by space-energy corrections to infinite media cross sections;
5. The use of a three-dimensional diffusion-depletion calculation to treat fuel and fission product isotopes and represent movable fuel;
6. A simplified P-3 transport calculation for the highest energy neutron group;
7. The use of three-dimensional coolant and fuel temperature feedback to the neutron distribution, which also takes account of cladding diametral shrinkage and fuel pellet growth;
8. The use of three-dimensional xenon feedback to compute the spatial flux distribution associated with equilibrium nuclide concentrations of iodine and xenon.

PDQ calculations for LWBR were performed in three-dimensional hexagonal-Z geometry; that is, the horizontal planar geometry had fuel rods on a triangular pitch so hexagonal fuel assemblies could be described. The detailed structure of the fuel rod cells (fuel pellet, cladding, support grid and coolant) did not

appear in PDQ neutron calculations. Homogenized fuel regions were represented by a three-dimensional mesh, used in the spatial flux solution, and by discrete three-dimensional "depletion blocks" which covered the fuel regions. A depletion block is a subregion such that nuclide concentrations are spatially constant over the block, but may vary from block to block as depletion occurs. Axial planes with a uniform spacing of 3-1/2 inches were used in the one-sixth core geometry to describe the core in the axial direction and to position the movable fuel seed modules. Thus, each spatial flux calculation could be done with the movable fuel position within 1.75 inches of the measured position.

Core performance depletion calculations, with the 1/6 core geometry in PDQ, contained 1472 transverse blocks each of which was divided axially into 3.5 inch segments. Of these 1472 blocks, 1390 were depletion blocks in fuel regions representing the 2883 fuel rod locations in the 1/6 core. Calculated nuclide inventories in the 1390 fuel blocks, following core depletion for 28,730 EFPH, form the basis for predicting LWBR fissile fuel content in all 17,290 fuel rods at end-of-life.

Transverse mesh spacings, used in PDQ spatial flux solutions, were smaller than depletion blocks and a total of 7055 (84 columns by 82 rows) transverse points were used in the 1/6 core geometry. Typical mesh widths in the 12 central modules were comparable to the fuel rod pitch, 0.37 inch in the seed regions and 0.63 inch in blanket regions. Wider mesh spacings were used in the low power peripheral reflector modules, 0.90 inch across the inner six rows of rods and 1.5 inches across the outer rod rows. Additional details of the PDQ three-dimensional geometry specifications are given in Reference 7.

LWBR burnup calculations were done with fuel depletion chains and fission product buildup chains in PDQ. The fuel chains included Th^{232}, Pa^{231}, Pa^{233} and U^{232} through U^{236}. Uranium fuel produced for LWBR fuel elements contained a small amount (less than 1/2 percent core average) of U^{238}. The U^{238} was not treated explicitly in a PDQ depletion chain, but its effect on the atom balance (for breeding analysis) was accounted for by a post-PDQ correction. Only a trace amount of plutonium will be present in the end-of-life fuel from U^{238} neutron capture, and no credit is taken for the plutonium in the calculated fissile fuel breeding ratio.

Four fission product chains were used, three of which accounted explicitly for the bulk of the poisons which depend on power level. The fourth chain accounted for all other fission products. The three explicit chains included xenon-135 and the bulk of promethium and samarium contributions, which provide about 50 percent of the total fission product absorption. Reference 7 contains additional details of the fuel and fission product depletion chains.

IV. LWBR NUCLEAR PERFORMANCE

Nuclear analyses of LWBR core performance consisted of two categories of calculations. One category was for reactor physics parameters measured during nine test periods. Tests were performed prior to power operation in September 1977, during seven periodic shutdowns from power and following the final October 1, 1982 shutdown. Results of this physics experimental program, presented in References 1, 2 and 3, have demonstrated that adequate margins were provided in safety analyses and that the calculational models provided generally accurate predictions of core behavior.

The other nuclear analysis category consisted of core depletion calculations for the power operation history of the entire 61 months of operation. Performance data for the LWBR core during power operation are presented in this section. These data include the power operation history in Section A, reactivity bias evaluation in Section B, breeding performance in Section C and power distribution data in Section D.

A. Power Operation History

LWBR operation from station startup (initial operation at power) on September 7, 1977 through final shutdown on October 1, 1982 accumulated 33,850 hours at power out of 44,410 total hours. The 10,560 hours with no electricity generation resulted from 85 outages of which 31 were of short duration for operator training. The 85 outages consisted of 68 which were shorter than three days (850 hours total), five in the three to eight day range (630 hours) and 12 including testing periods which were longer than eight days (9080 hours total).

Nuclear analysis core follow depletion calculations, which approximated the operating history, began after an initial (time zero) spatial flux and power calculation was performed, with thermal feedback, using the three-dimensional one-sixth core PDQ model. The procedure called thermal feedback provides the capability to compute a spatial flux distribution which is consistent with the spatial distribution of fuel temperature, moderator temperature, and moderator density. This feedback procedure consists of first calculating the power (flux) distribution, assuming some temperature and moderator density distribution, and then calculating temperature and density distributions based

on this power distribution. A new power distribution is then calculated using the latest temperature and density distributions. The initial spatial flux calculation for LWBR (zero depletion time) contained uniform temperatures and moderator density and was followed by two iterations of temperature feedback. Subsequent calculations, referred to as "timesteps", consisted of:

1. Depletion from time T_1 to T_2 using the spatial flux distribution from the previous timestep at T_1 and holding it constant in time;
2. Upward motion of the movable fuel to a new measured fuel position; and
3. Spatial flux calculations including one recalculation of temperature and xenon distributions.

The LWBR depletion history consisted of 57 timesteps, shown in Figure IV-1, including 48 at-power timesteps plus nine zero power timesteps. An average power level was used during each calculation such that both real time and EFPH were maintained consistent with core operation. The average timestep length was about 600 EFPH (28,730 EFPH/48). Time at zero power is important for a core with thorium fuel because of protactinium-233 buildup while at power, which decays to U-233 with a half life of 27 days. Thus, the nine zero power timesteps shown in Figure IV-1 included all 12 outages longer than eight days plus a few contiguous or nearly contiguous short outages for a total of 9317 hours. The remaining 1243 hours at zero power from short shutdowns were included as part of the at-power time to reduce the number of zero power timesteps for calculational simplicity.

LWBR operation at nominal full power of 236.6 MW (thermal) corresponded to 72 MW electric gross and 60 MW electric net. The power producing volume (based on 12 fuel modules, and an 84 inch binary fuel height) was 4,430 liters, yielding a core power density of about 53 KW (thermal)/liter.

A summary of LWBR power operation is presented in Table IV-1 for the 61 months of operation shown in detail in Figure IV-1. These operation data are reported for 1) design lifetime through 18,298 EFPH, 2) extended lifetime of 10,432 EFPH and 3) total lifetime of 28,730 EFPH. The LWBR core average depletion in the power producing core volume was equivalent to about 14,600 MWd/t over the total operating lifetime which produced 2.10 billion kilowatt hours electric gross and 1.70 billion kilowatt hours electric net during 61 months of operation.

The plant generated power for 33,850 hours. The total availability factor (100 x hours plant generated power/total hours) was 76.2% and the overall capacity factor (100 x net MWh/design electric rating x total hours) was 64.0 percent.

The capacity factor was 70.2% and availability was 74.7% during the design lifetime of LWBR (18,298 EFPH). These factors were lower than expected due largely to unanticipated time spent confirming the safety assessment after discovery of a larger-than-expected flow coefficient during the Spring, 1979 tests (References 2 and 3). A larger availability factor of 78.5% was obtained during the extended lifetime. The lower capacity factor of 54.9% during the extended lifetime period was due to reduced maximum power level operation specified to reduce duty requirements on core and plant components and to provide additional reactivity lifetime during the additional two years of

operation. In addition, the end of reactivity lifetime at a maximum power level of 80% was reached at about 27,100 EFPH, with the 12 movable seed assemblies at the maximum withdrawn position, and a further extension in lifetime of about 6% was obtained by a gradual power coastdown to 57% power prior to the final shutdown at 28,730 EFPH.

The lifetime average power level was 84.9% during time at power. The 92.7% level during the design lifetime included 204 planned swingloads during which power was reduced to between 60 and 35 percent for periods of from four to eight hours. Planned swingload cycles were performed to demonstrate fuel element and plant capability to accomodate representative load follow demand during typical utility operation. There has been no indication of fuel element failure based on radiochemical sampling of the reactor coolant.

The nuclear analysis power history approximations, shown in Figure IV-1, include 1243 hours of short outages which increased the at-power time in depletion analysis from 33,850 hours to 35,093 hours. This resulted in a lifetime average power level (while at power) of 81.9% which is about 3 percent below the 84.9% obtained from actual power operation. The total energy output for each depletion timestep matched actual operation.

Measured movable fuel positions during core lifetime power operations are shown in Figure IV-2. Representative data points which are sufficient to show the general variation in movable fuel position throughout lifetime are given in Figure IV-2. For each depletion interval in the core follow calculations, the movable seed assembly bank was positioned at the axial mesh point nearest to the average measured position during the interval. Movable fuel bank positions for the at-power depletion calculations are also shown in Figure IV-2. The axial mesh requires axial moves in increments of 3-1/2 inches.

Station startup at beginning-of-life consisted of low power testing followed by about 2 days at 67%-70% power, during which the movable fuel position increased from about 36 to 39 inches. Then power was gradually increased during 5-1/2 days to achieve 100% power, with a movable fuel position of 41.5 inches (details are in Reference 1). The rise in critical bank position was due both to the direct effect of power increases (i.e., the Doppler effect in thorium) and to the increase in xenon poison content. Buildup of samarium and protactinium also caused a relatively large rate of decrease in reactivity and thus a relatively rapid fuel motion for the first 2000 to 3000 hours at high power.

Typical LWBR reactivity coefficients, measured at normal operating conditions, are presented in Table IV-2 for changes in power level, temperature and pressure. The magnitudes of these coefficients are averages of measured data between beginning-of-life and 18,298 EFPH (see Reference 2). Reactivity worth of equilibrium xenon was measured near beginning-of-life (1.83×10^{-2} $\Delta\rho$/100% Xe) and at 18,298 EFPH (1.49×10^{-2} $\Delta\rho$/100% Xe). The typical value (1.66×10^{-2} $\Delta\rho$/100% Xe), in Table IV-2, is an average of the two measured xenon worths. Decay of protactinium-233 to U-233 removes a neutron absorber from the core and also increases the fissile fuel content; both effects increase the core reactivity. The reactivity worth of full-power equilibrium Pa-233 measured at 10,771 EFPH (Reference 11) was 2.45×10^{-2} $\Delta\rho$/100% Pa, as given in Table IV-2. As reported in Reference 11, Pa-233 reactivity worth decreased with lifetime; a worth of 2.05×10^{-2} $\Delta\rho$/100% Pa was inferred from measurements following 18,298 EFPH of operation. Reductions in measured fuel position shown in Figure IV-2, which occurred following each periodic shutdown, were due to reactivity in-

creases from decay of xenon and protactinium. Changes in fuel position due to variations in power level, temperature and pressure were relatively small and the measured positions in Figure IV-2 were chosen for nominal conditions close to full power.

Movable fuel reactivity worth (10^{-4} $\Delta\rho$/inch) as a function of movable fuel position, calculated at selected times during power operation, is presented in Figure IV-3. The fuel worth decreased from about 40 x 10^{-4} $\Delta\rho$/inch near beginning of life, with the movable fuel bank at about 41 inches, to around 4 x 10^{-4} $\Delta\rho$/inch at end-of-life with the movable fuel close to the fully withdrawn (84 inch) position. The low fuel worth for higher positions of the movable fuel was the major contributor to the rapid rise in the movable fuel position toward end-of-life, shown in Figure IV-2.

B. Reactivity Bias Evaluation

Reactivity calculations were performed at the end of each depletion interval in the core follow sequence by adjusting the three-dimensional sixth-core PDQ power from the average power in the time step to the instantaneous core power. Xenon feedback was used to set the xenon level to the equilibrium level consistent with the instantaneous power level. Depletion intervals were chosen such that the power level, and thus the xenon level, was nearly constant near the end of each interval. Single iterations of temperature feedback, which included the time integrated fuel pellet growth and cladding shrinkage effects, were also employed to update the core temperature distributions to be consistent with the power distribution at this time. Generally, two eigenvalue calculations

were done for each time with different movable fuel positions (3.5 inches apart) to obtain a calculated movable fuel bank worth.

The sixth-core calculated reactivity bias at each core follow depletion interval, or "checkpoint", was determined by comparing the corresponding calculated eigenvalue to the design model critical eigenvalue following adjustments for:

1. the difference in movable fuel bank height between the PDQ calculation at the nearest axial mesh point and the measured height. Calculated bank worths were used to convert the height difference to a reactivity effect.
2. the difference in measured average coolant temperature and the PDQ average temperature (531°F up to 18,298 EFPH, 521°F after 18,298 EFPH). The PDQ calculated total, fuel plus moderator, temperature coefficient was used for this conversion.
3. the difference in measured coolant pressure and the pressure used in PDQ (2000 psia up to 18,298 EFPH, 1600 psia after 18,298 EFPH) using the measured pressure coefficient of reactivity.
4. the difference in xenon between the equilibrium level associated with the checkpoint power level and the level that would apply due to the previous power history. Checkpoints were purposely chosen such that in most cases the core had run for about 40 or more hours at nearly constant power. Thus this correction was generally less than 0.04% $\Delta\rho$ and for many checkpoints was zero. Point depletion codes were used to calculate the relative xenon levels at checkpoints during periods when xenon was not in equilibrium.

5. the use of a constant residual fission product cross section in PDQ which overestimated the fission product absorption by a small amount during the first few thousand EFPH.

In addition to the sixth-core bias corrections, a coarse-to-fine depletion time step correction was obtained using an R-Z geometry PDQ model for a central (Type I) seed-blanket module. Two R-Z calculations were done throughout lifetime. The coarse time step calculation followed the core power history in the same detail as the sixth-core depletion with respect to power level, fuel height, time step length, and xenon-temperature feedback scheme. The fine time step calculation utilized approximately four times as many time steps, and average fuel heights, and multiple feedback calculations. The reactivity difference between these two calculations was determined at each core-follow checkpoint by performing similar checkpoint calculations at the same conditions (power level, temperature, pressure, xenon state) as the three-dimensional checkpoint calculation. This difference was then used to correct the core-follow bias.

The behavior of the reactivity bias is presented in Figure IV-4 which shows the percent reactivity excess of experiment over calculation through lifetime. Results are shown for full power conditions and also for hot zero power and cold conditions obtained during periodic testing (discussed in References 1, 2 and 3). Bias results show that the core was more reactive than calculated at full power and that the bias showed a generally increasing trend during lifetime. Following the third periodic shutdown at 10,771 EFPH, the core follow reactivity bias at power decreased from 0.38% $\Delta\rho$ to 0.26% $\Delta\rho$ overreactive. This loss of reactivity is consistent with the larger-than-expected increase in the flow coefficient of reactivity observed at the same shutdown and

which was discussed in References 2 and 3. After 10,771 EFPH, the core follow reactivity bias increased to a maximum of 0.54% $\Delta\rho$ overreactive late in core life. The coarse-to-fine depletion time step correction varied between -0.04% $\Delta\rho$ and +0.04% $\Delta\rho$ throughout lifetime.

The reactivity bias for all measured conditions, shown in Figure IV-4, was well within the off-nominal reactivity allowance of ± 1% $\Delta\rho$ used in predicting the lifetime performance and safety aspects of LWBR (Reference 16). The basis for the ± 1% $\Delta\rho$ off-nominal reactivity allowance is discussed in Reference 6. The small reactivity bias was achieved without the benefit of a full scale mockup critical or of any similar previous core.

1. Effect of Fission Product Data on Reactivity

One possible component of the bias is overestimation of fission product absorption. Several calculations were performed using the ENDF/B version IV fission product data (Reference 12), which is newer than that which was used in LWBR core follow analysis (Reference 7). The ENDF/B-IV fission product data indicate reduced neutron absorption as the core depletes compared to the fission products in the LWBR calculational model. A one-point CINDER (Reference 13) depletion calculation was performed using the ENDF/B-IV fission product data and the 84 nuclide chain CINDER from Reference 12. The calculated total epithermal fission product absorption was about 19 percent smaller than that calculated using the design model (Reference 7) throughout lifetime. Total calculated thermal fission product absorption was also smaller using the ENDF/B-IV calculations compared to the design model. The difference in fission product thermal absorption increased through lifetime from 1.2% early in life (3000 EFPH) to about 4% at end-of-life.

An R-Z geometry PDQ model calculation for a central Type I seed-blanket module was also performed using the ENDF/B-IV fission product cross section data. This calculation included core depletion to about 40 percent of core lifetime (11,000 EFPH). The difference in PDQ calculated reactivity from the reference design model PDQ was minus 0.008% $\Delta\rho$ at 100 EFPH, but increased to plus 0.24% $\Delta\rho$ at 5,000 EFPH and to plus 0.44% $\Delta\rho$ at 11,000 EFPH. The small negative reactivity effect at 100 EFPH is due to a slightly larger (about 1.4%) calculated xenon-135 absorption using the ENDF/B-IV data.

Fission product absorption fractions from the Type I module PDQ calculations at 11,000 EFPH, with ENDF/B-IV versus design model fission product cross section data, were larger by 1.4% for xenon-135, smaller by 9.0% from the two chains with promethium and samarium nuclides, and smaller by 14% for the other (residual) fission products. The cumulative effect for all fission products was an 8.6% smaller absorption fraction with ENDF/B-IV fission product data than with design model data. Subsequent analysis of fission product poisoning in the LWBR core neutron spectrum using the even newer 102 chain ENDF/B-V fission product data show less than 1% increase in neutron absorption in fission products relative to ENDF/B-IV. The LWBR fission product cross sections were qualified against irradiation experiments and did well in predicting those experiments (Reference 7 and other references cited there). Thus it is not certain that ENDF/B-IV is better. At this time, it is not known what contribution the fission product treatment is making to the bias, but the fact that the ENDF/B-IV and ENDF/B-V fission product treatments lead to a much smaller reactivity bias change for the LWBR core implies that these newer, more detailed data are better than the original LWBR set.

2. Clad Shrinkage and Fuel Swelling Effects on Reactivity

Another possible component of the reactivity bias is cladding diameter shrinkage and fuel swelling calculational uncertainties. The LWBR model (Reference 7) includes the explicit calculation of thermal conductance of the fuel-cladding gap taking into account cladding diameter shrinkage due to fast-neutron-induced creep, fuel pellet contraction due to densification, fuel pellet expansion due to fission product induced swelling and thermal expansion, and changes in the conductivity of the gas in the gap due to release of noble gas fission products. The purpose of including these factors was to provide more accurate calculations of fuel temperature and determinations of the water content which affects core reactivity. The fuel lattice water volume changes because of the change in coolant channel cross sectional area caused by cladding diameter changes due to either shrinkage or expansion.

Cladding shrinkage and fuel pellet expansion both reduce the size of the fuel-cladding gap, thereby increasing thermal conductance and resulting in lower fuel temperature. Core reactivity is increased when fuel temperature is reduced due to changes in the Doppler-broadened cross sections. Cladding shrinkage also increases the coolant channel area and thus the hydrogen concentration in the fuel lattice, which also causes an increase in core reactivity. Conversely, cladding diameter increase due to outward pressure of the expanding fuel after the gap disappears decreases the hydrogen concentration in the fuel lattice and causes a decrease in core reactivity. For the LWBR seed rods this latter effect is unlikely since the seed rods had free standing cladding and an as-built radial pellet-cladding gap thickness of 4.95 mils averaged over the

binary fuel. Standard blanket and power-flattening blanket rods however had non-free standing cladding and as-built average radial gap thickness of only 2.5 mils, and some cladding diameter increase was predicted to occur in these fuel regions.

Approximations made in the PDQ calculational model for treatment of the factors outlined above are presented in Reference 14, which also shows the calculated magnitudes of changes in fuel temperature and pellet and cladding dimensions for LWBR rods. Typical decreases in cladding radius for standard blanket and power-flattening blanket rods are about 2 mils, and increases in the cladding radius occur at various times, as early as 2,000 EFPH. The change in radius of seed rods is rather gradual, about 1/2 mil in 18,000 EFPH, compared to that of blanket rods, due to the smaller ratio of outer diameter to clad thickness (and hence lower hoop stress) in the seed rods.

Testing of the PDQ cladding shrinkage and fuel pellet swelling model by comparison with more detailed, explicit calculations using the CYGRO-4 analysis procedure (Reference 15) was presented in Reference 14 for the 18,000 EFPH core design lifetime. Continuation of these studies for extended LWBR core lifetime (beyond 28,000 EFPH) showed generally good agreement on fuel temperature calculations but the cladding radii were "overpredicted" by the model late in life (i.e., the model in PDQ predicted too large a radius). The amount of overprediction was small ($\approx$ 0.1 mil) for seed rods but averaged about 0.5 mil throughout the blanket regions of the core. The effect of this overprediction is estimated to reduce the PDQ calculated reactivity by about 0.12% $\Delta\rho$ and thus this effect may account for about one-fourth of the observed reactivity bias late in core life.

C. Breeding Performance

Reasons why breeding can be achieved in a light water reactor using the uranium-233/thorium fuel system are presented in Reference 4. Performance parameters measured during LWBR core operation do not provide direct information on the amount of fertile material transformed into fissile fuel. Breeding performance was predicted using the LWBR calculational model and will be confirmed by fuel rod assay of about 500 rods taken from selected modules to determine the end-of-life fissile content of the core (Reference 17). An extensive proof-of-breeding program is underway to do non-destructive evaluations at the Idaho National Engineering Laboratory, and destructive evaluations at Argonne National Laboratory. But overall good model performance (reactivity bias, etc.) provides confidence that LWBR did breed.

1. Calculation of Breeding Parameters

Breeding parameters for the LWBR were evaluated at the end of each depletion interval during the depletion history shown in Figure IV-1. The quantities which describe breeding performance are the conversion ratio (CR) and fissile inventory ratio (FIR). The conversion ratio is the ratio of instantaneous fissile production rate to instantaneous fissile destruction rate. The FIR is the ratio of fissile inventory at a given time in core life to the initial fissile inventory built into the core and is a time integral which depends on the conversion ratio. When FIR exceeds 1.0 (plus estimated recycle losses) the core is a net breeder. Definitions of these quantities and their

relationship to nuclear reactions, derivation of equations for calculating breeding, and the relationship between conversion ratio and fissile inventory ratio are presented in detail in Reference 6 and summarized below.

There are two basic quantities that determine the CR. One is the value of η (neutrons produced per neutron absorbed) of U^{233}, and the other is the neutron capture competition between thorium and parasitic materials. Since the reactor is critical at some power level, for every neutron absorbed by U^{233}, there are η-1 neutrons remaining which are shared among thorium, water, cladding, structure, and the products of depletion. The fraction of the remaining neutrons which thorium absorbs determines fissile production rate.

Calculated breeding parameters for LWBR are presented in Figure IV-5 for both a hypothetical continuous 100 percent power operation and for the actual core operating history. The upper figure shows the conversion ratio. At beginning-of-life the conversion ratio is at its maxium value and is greater than 1. As the core depletes and protactinium-233 and fission products build up, the conversion ratio decreases with lifetime. However, the conversion ratio is enhanced during periods of core operation at less than full (100 percent) power and following periods at zero power, due to a reduction in xenon-135 and protactinium-233 concentrations. When the coversion ratio reduces to unity late in core life, the fissile content of the core is at its maximum.

Conversion ratio (CR), at time t, is defined by

$$CR(t) = \frac{\text{instantaneous production rate of fissile atoms at time t}}{\text{instantaneous destruction rate of fissile atoms at time t}}.$$

Substituting the fertile and fissile nuclides, the equation becomes

$$CR(t) = \frac{C^{Th\text{-}232}(t) + C^{U\text{-}232}(t) + C^{U\text{-}234}(t) + A^{Pa\text{-}231}(t)\left(\frac{F^{U\text{-}232}(t)}{A^{U\text{-}232}(t)}\right) - A^{Pa\text{-}233}(t)}{F^{U\text{-}232}(t) + A^{U\text{-}233}(t) + A^{U\text{-}235}(t)}$$

where

$C^i(t) = A^i(t) - F^i(t)$ denotes capture rate in nuclide i at time t,

$A^i(t)$ denotes absorption rate of nuclide i at time, and

$F^i(t)$ denotes fission rate of nuclide i at time t.

The nuclides Th-232, U-232, Pa-231, U-234 are considered to be "fertile material" since upon neutron capture they are converted to fissile material. The fraction of U-232 which fissions is treated as fissile fuel. The assumption that Pa-231 does not fission is implicit in Equation (2). Available nuclear data for Pa-231 support this assumption.

The fissile inventory ratio was computed by integrating the conversion ratio over time; that is, the change in FIR between times t_1 and t_2 is

$$\Delta FIR(t_1 \rightarrow t_2) = \left[\frac{A_f(t_1) + A_f(t_2)}{2\,N_0}\right] \left[\frac{CR(t_1) + CR(t_2)}{2} - 1\right] (t_2 - t_1) ,$$

where A_f is the absorption rate in fissile material and N_0 is the initial number of fissile atoms in the core. Then, the FIR at any time t_n is

$$FIR(t_n) = 1 + \sum_{i=1}^{n} \Delta FIR(t_{i-1} \rightarrow t_i) .$$

Fissile inventory ratio, shown in the lower figure on Figure IV-5, continues to increase until the conversion ratio is less than 1.0, after which FIR starts to decrease. The solid line shows the calculated FIR based on an

assumed continuous 100 percent power operation. Calculations for actual power operations indicate a peak FIR of 1.015 at about 22,300 EFPH and a predicted FIR of 1.013 at the end of core operation at 28,730 EFPH. The FIR at the end of 100% power, 18,300 EFPH, was slightly higher than at end-of-life. The reduced power in the extended lifetime period partially compensated for the increase in fission products. Thus an additional 10,000 EFPH was obtained with only a small reduction in FIR.

The effect of fission product data was discussed in Section IV.B.1 as a possible contributor to the reactivity bias. Data presented in Reference 6 shows the large effect of neutron losses to fission products on the conversion ratio. If the actual fission product absorption was less than the calculated absorption, then thorium neutron absorption would be larger. An increase in thorium absorption would produce more U-233 and result in a larger fissile inventory ratio than calculated.

2. Fissile Fuel Distribution Changes

Total core fissile loading throughout core lifetime remains within 2 percent of the initial loading. There is however a shift with time in U-233 spatial density between seed regions and blanket regions. Figure IV-6 shows the calculated fissile loadings in the total seed, standard blanket, power-flattening blanket, and radial reflector region, summed over the entire core, as functions of time. The 20 percent reduction in total seed region fissile loading is due to depletion resulting from the large excess reactivity required in the seed region to achieve adequate lifetime from the batch-loaded LWBR core.

However, the net increase in blanket and reflector region fissile loading more than compensates for the reduction in seed region loading.

As a function of time, U-233 depletion generally decreases the U-233 content in most binary regions, but neutron absorption in Th-232 results in a buildup of U-233 in thoria regions. A comparison of the beginning- and end-of-life fissile loadings in all 12 fuel compositions is given in Table IV-3. High-zone, medium-zone and low-zone refer to the relative amount (w/o) of U-fissile present in various fuel rods. Specifications and locations of these binary fuel regions were presented in Reference 6. A comparison is presented in Table IV-4 showing calculated fissile loadings in seed, standard blanket and power-flattening blanket regions in each module type both at beginning- and end-of-life.

Local variations in U-233 spatial density occurred slowly due to the simultaneous depletion of U-233 and the production of U-233 by neutron capture in Th-232. The largest net changes in U-233 loading per rod are in the high-zone seed rods, about 26 percent on the average, and in the high-zone power-flattening blanket rods, about 14 percent in an average rod (see Table IV-3). High-zone standard blanket rods have a smaller change, about 4.5 percent in an average rod. Calculated axial distributions of U-233 at end-of-life are shown in Figure IV-7 for the binary length of highly depleted seed, standard blanket, and power-flattening blanket high-zone rods.

The net change in U-233 loading within the low-zone seed (31 percent) is about the same as in the high-zone seed, but production of U-233 in the thoria portion of these rods (see Table IV-3) results in an average loading per rod only about 10 percent below the initial loading. A comparison of the

calculated axial distribution of U-233 at beginning-of-life and end-of-life in a typical 42-inch binary seed rod (outer two seed rows shown in Figures II-2 and II-3) is shown in the upper graph on Figure IV-8. Calculated end-of-life U-233 loadings for the blanket and power-flattening blanket rods closest to the seed assemblies, low-zone and medium-zone in Rows 1 to 3 (see Figure II-3), exceed the initial loading. A comparison of the axial distribution of U-233 at beginning- and end-of-life for an average 42-inch binary standard blanket rod in the Type I module, given in the lower graph on Figure IV-8, shows a buildup of U-233 in both the binary and thoria segments of the rod.

Buildup of U-233 in the reflector blanket regions, module Types IV and V (see Figure II-1) is larger in the inner rod rows than in the outer rod rows. At end-of-life, the total U-233 content in all 3047 reflector rods is calculated to be 37.8 kg, or an average of about 12.4 grams per rod. The calculated U-233 content for the 516 rods in the first two rod rows is 13.6 kg, or about 26 grams per rod. Thus, the first two rows of rods, which contain 17 percent of the total reflector rods, contain 36 percent of the U-233 content in the reflector. The largest U-233 content is calculated to be about 40 grams in the reflector rod located at the apex of the Type IV module. The calculated U-233 axial distribution in this rod at end-of-life is shown in Figure IV-9.

D. Power Distribution and Power Performance Data

The power operation history and total LWBR core depletion were discussed in Section IV.A and summarized in Table IV-1. Radial and axial power distributions have been calculated throughout core life using the explicit

three-dimensional sixth-core block depletion PDQ model discussed in Section III. These calculations include directly the feedback effects of three-dimensional distribution of fuel and moderator temperature in the core and effects of fuel swelling and fuel rod cladding diameter shrinkage.

1. Gross Radial and Axial Power Distributions

Figure IV-10 shows the calculated power fractions in gross regions of the core as a function of time in core life. The percent of core power is given for the total seed, standard blanket, power flattening blanket, and radial reflector regions. Relatively flat gross radial power shapes were maintained throughout life. Upward positioning of the movable seed assemblies above the aligned position later in core life, as well as depletion effects, resulted in a decrease of only ten percent in seed power fraction from about 39 percent of core power near beginning-of-life to 35 percent at end-of-life.

Fractional contributions to core power from each region in each module type (location of each module type is shown in Figure II-1) are presented in Table IV-5 for three times in core life.

The LWBR core, with a pressure vessel inner diameter of 109 inches, was much smaller than the core in a large central station commercial reactor plant. A small diameter core generally has large radial neutron leakage and larger power peaking at the center of the core. The presence of the reflector blanket modules, to reduce radial neutron leakage from the core, leaves an effetive diameter for the 12-module power producing region of the core of approximately 68 inches. The LWBR core was therefore designed with a peripheral "power-flattening blanket" region, shown in Figure II-1, to reduce power

peaking in the central modules. These design features for the small LWBR core better simulate in the three central (Type I) modules the breeding environment of a large core. This power-flattening blanket region contains 10 rows of rods, compared with 6 rows in the inner "standard blanket". It has a larger U-233 content in the fuel and a smaller metal/water ratio than the standard blanket region.

Calculated power distribution data presented in Table IV-5 show that both the three central Type I modules and the three Type II modules each produce about 8.5 percent of core power while each of the six Type III modules contribute about 8 percent of core power. The power density however is somewhat larger toward the core center. For example, the 18,300 EFPH data in Table IV-5 show that the ratio of power in a Type I seed to power in a Type II seed is 1.13 and the ratio of power in a Type II seed to power per Type III seed is 1.12.

The calculated axial power distribution is skewed toward the top of the movable seed assemblies early in core life and toward the bottom late in core life. This effect is shown by the data presented in Figure IV-11 for four 21-inch axial zones in the 84-inch binary fuel height. The variation in axial power distribution with lifetime is much less pronounced in the blanket regions than in the seed assemblies. Data in Figure IV-11 show that the central 42 inches (Zones 2 plus 3) in both the blanket and power-flattening blanket (PFB) account for about 64 to 74 percent of the region power. Note that the core conditions for axial power data, in Figure IV-11, are exactly the same as for the power data by module and regions, presented in Table IV-5.

Calculated heat flux (Btu/hr-ft^2), linear power density (kw/ft) and fuel depletion data (fission/cm^3 and megawatt days per metric ton (MWd/t) of thorium plus uranium) are presented in Table IV-6. Note that the maximum levels given in Table IV-6 include the allowances and uncertainty factors discussed below in Section IV.D.3. The region averages and the local maxima of heat fluxes and of linear power densities are presented in Table IV-6 for seed, blanket, and power-flattening blanket at 100 EFPH and for the reflector blanket at about 27,000 EFPH, at which time significant buildup of U-233 has occurred in the reflector blanket. All heat flux and linear power density data in Table IV-6 have been normalized to 236.6 MWth. Region average and local maximum fuel depletion data are given in Table IV-6 for both 18,300 EFPH (the design lifetime) and for end-of-life (28,730 EFPH).

2. Local Power Distributions

The LWBR core was designed to be operated and controlled with all movable seed assemblies positioned in a uniform bank. Acceptable power distributions were designed into the core by means of the radial and axial fuel zones and the specified U-233 content in each region of the core, as described in Reference 6. As a result, no operational procedures were required to shape or alter radial or axial power distributions by control element programming during full-power operation.

On the few occasions when the core was both xenon free and nearly protactinium free, such as during return to power operations following the long shutdowns shown in Figure IV-1, operation at less than 100-percent was required. Under these conditions, with the movable fuel bank position low in the core

relative to the seed-blanket aligned position (see Figure IV-2), calculated local power peaks were considerably larger than prior to the shutdown. Thus, to ensure acceptable fuel element and thermal/hydraulic performance, operation at about 20-percent below full power was specified for about one-to-two days until the xenon and protactinium content were sufficient to raise the movable fuel bank to a position where the calculated local power peaks were acceptable. This type of power level restriction happened only after long shutdowns because of the 27 day Pa-233 half life.

The LWBR core power distribution never experienced xenon-induced oscillations. A large margin of stability was shown by the analyses presented in References 6 and 18. A test was also performed at 15,000 EFPH to confirm the stability of LWBR against xenon-induced power oscillations. Parameters depicting stability characteristics of a ^{233}U-Th reactor were measured and found to agree with predictions (Reference 19). Those predictions indicate that even a large size LWBR would be stable against xenon-induced power oscillations.

Axial power distributions are shown in Figures IV-12 through IV-15 where heat flux, in units of Btu/hr/ft^2, is plotted for the entire fuel stack length. The data represent the averages of pointwise power calculated from four PDQ mesh points for each rod at each axial PDQ plane (spaced at 3.5-inch increments) for the core at 100-percent power. Data for a high depletion high-zone seed rod, in rod row 11 of the Type I module, are given in Figure IV-12 for three times in core life: (1) near beginning-of-life, with equilibrium xenon, when the seed assemblies were displaced downward relative to the blanket assemblies, (2) at 18,300 EFPH when seed and blanket assemblies were axially aligned, and (3) near end-of-life when the seed assemblies were displaced upward relative to the blanket assemblies. These fuel positons are shown schematically

in Figure IV-11. As a function of time, as the seed fuel assemblies moved upward in the core, the location of the axial power peak shifted from the upper portion of the rod to the lower portion during lifetime. Note that the near end-of-life heat flux in Figures IV-12 through IV-15 are relative shapes only, since the actual heat flux after 18,300 EFPH was reduced by the lower power operation (see Figure IV-1).

Figure IV-13 shows similar axial power distribution data for a high depletion high-zone standard blanket rod in the Type I module. Power was concentrated in the lower two-thirds of the rod near beginning-of-life, when the seed assemblies were displaced downward relative to the blanket assemblies, and in the upper two-thirds of the rod near end-of-life when the seed assemblies were in the raised position.

The relatively large water gap between the outer rod row in the seed assembly and the inner rod row of the blanket assembly (see Figure II-2) causes a peaking of the thermal neutron flux in this region. Fuel rods near the seed-blanket interface were loaded with low-zone (lower U-233 content) fuel so that the local power peaks would be more nearly comparable to the power peaks in the high zone fuel rods located in internal rod rows which have less water moderation.

Axial power distributions in a low-zone seed rod, shown in Figure IV-14, are similar over the 42 inch binary length to the power distributions in the high-zone seed rod (Figure IV-12). Likewise the axial power levels in the 42 inch binary length of a low-zone blanket rod, shown in Figure IV-15, are similar to power distributions in the high-zone blanket rod (Figure IV-13).

Also shown in Figure IV-15 is a sizeable heat flux in the ThO_2 segment of the low-zone blanket rod at 18,300 EFPH and near end-of-life. This is due to the large build-up of U-233 in the ThO_2 stack length shown in the lower figure on Figure IV-8.

Data given on Figures IV-12 to IV-15 show that the maximum local heat fluxes in the seed and blanket regions are largest at beginning-of-life. The heat fluxes in these regions decrease sharply during early-in-life full-power operation. The LWBR core local power peaking factors (ratio of maximum local power to region average power) are, therefore, largest at beginning-of-life. Peaking factors of local heat flux and maximum rod power at the beginning-of-life and depletion peaking factors near end-of-life are presented in Table IV-7 for the seed, standard blanket, and power-flattening blanket regions. These peaking factors include the allowances and factors presented in Section IV.D.3. The power late in life in hottest reflector rods was a core performance concern, just as the power in the seed and blanket rods (Table IV-6); but the notion of a peaking factor is not useful because the fall-off in power or depletion toward the outside of the reflector is so great that the region average is very low and of little interest.

3. Allowances in Power Performance Data

Local pointwise power data and rod power data obtained from the three-dimensional PDQ calculations for LWBR were adjusted by several power allowance factors. Conservative factors were used for setting core operating limits and for core performance analyses (see References 6, 7, and 16) to

provide assurance of satisfactory fuel element and thermal/hydraulic performance. Allowances were included for uncertainties in the nuclear analysis model, for manufacturing tolerances including fuel misalignment, and for variations anticipated during core operation including instrumentation errors. A large contribution to these factors was from the experiment-to-calculation allowance which was based on detailed comparisons of power distributions calculated using the LWBR model with those power distributions measured in a variety of experimental configurations. The experimental configurations are discussed in detail in References 20 and 21, and the development of experimental-to-calculation correction factors is discussed in References 6 and 7. All of the experiments contained $U^{233}O_2$-ThO_2 loaded fuel rods but were much smaller and/or simpler cores than the LWBR core. The BMU experimental series consisted of 3 single module and 3 multi-module configurations of the seed-blanket type, with active fuel lengths of 28 inches for seed rods and 42 inches for blanket rods. The Detailed Cell series consisted of 7 experiments involving a single Type II module surrounded by a varying number of additional fuel rods known as the driver. The seed was positioned at a different height relative to the blanket in each case and the amount of driver was varied with seed height to maintain criticality. Satisfactory LWBR core operation for 28,730 EFPH with no evidence of fuel element failure has shown that the power allowance factors were sufficiently conservative.

Core evaluation following disassembly of the core will consist of core component examination and proof-of-breeding (Reference 17) programs. To make predictions of core component conditions following irradiation for 28,300

EFPH, conservative factors are inappropriate and best estimate correction factors are needed. It is not appropriate to use the Detailed Cell measurements (Reference 21) for a best estimate core examination because the Detailed Cell was a beginning-of-life module and also because the Detailed Cell was a single module with a driver. Following is a discussion of best estimate power allowance factors, which are presented in Table IV-8.

The approach taken for postirradiation core evaluation was to use measurements from the periodic physics tests. These periodic tests (References 1, 2, 3) and the core follow reactivity bias indicate that the nuclear analysis model has provided a reasonably accurate description of the core. The radial symmetry data indicate the power in a module compared to the power in another module of the same type. These data are available for all modules at several times in core life. Interpreting the data depends on the approximation that the relative power in a module is proportional to the square root of the reactivity worth in a small bump from critical (Reference 1). Table IV-8A has lifetime averages of the symmetry measurements. This set can be used to adjust the power in a module compared to that in another module of the same type. The range is 0.994 to 1.006 so the effect is small.

The other core measurements which give power data are the flux wire irradiations. Axial activation shapes are available throughout life at flux wells located in the outer part of 7 blanket assemblies and one reflector. Integrations of the activation shapes axially provide information on the radial activation distribution. The flux wire activators were copper and nickel. Copper is a thermal and epithermal activator and was used to represent power. Averaging the flux wire activations by module type and then averaging over life-

time gave factors (Table IV-8B) to adjust power in one type of module relative to that in another. A large reflector module factor (1.13) occurs at the Type IV flux well located far from the power flattening blanket (in rod row 7 out of 10) toward the module outer boundary. The poor results in the Type IV reflector are believed to be primarily caused by a wide mesh spacing (discussed in Section III) and a crude geometric representation in PDQ of the region near the reflector outer boundary, which had to be represented by a jagged line in PDQ. For rods near the Type IV apex, an experiment-to-calculation factor (E/C) ≈ 1.00 is more appropriate because of their proximity to the central 12 modules which have a flux wire E/C of about 1.0. An intermediate factor between 1.0 and 1.13 will be assigned to other rods between the apex rod and the flux well in Type IV reflector modules, and also in Type V modules.

Power allowance factors established for fuel rods adjacent to the module support posts are given in Table IV-8C. The seed post rod E/C factor of 1.066 is based on a Detailed Cell experiment but has been retained because it is dominated by the local post geometry rather than by depletion or gross core geometry. For the same reason, blanket post rod E/C factors of 0.95 and 0.98 on power have been retained from a beginning of life RCP (Reference 2?) vs PDQ calculation. No post rod factors for the reflector are available. Since these reflector rods have low power, the E/C factor is less important.

No rod currently intended for examination is adjacent to a flux well. Detailed Cell experiments indicate a power increase of 2% to 4% (Reference 21) if such a rod should be chosen in the future.

The most important part of the axial shape experiment-to-calculation factor is due to the grid homogenization in the PDQ model. In PDQ, the fuel rod support grids made of AM-350 stainless steel are homogenized radially and

axially. At grid locations, the reduced water volume causes a dip in power. The grid dip factors in Table IV-8D were obtained from measurements in Reference 21 and from LWBR core flux wire activation data (References 2 and 3). Since the power shape dips in the grid region, it rises above the PDQ (homogenized grid) value between grids. A power allowance factor of 1.03 was established from measurements in Reference 21 to account for power peaking between grids. The actual factor determined from flux wire data varies with position and time as does the grid dip.

Factors to account for variation in U-233 loading of fuel pellets can be obtained from as-built loading data for any rod. All fuel pellet (local) factors are less than 1.3% in the seed and 1.0% or less in blanket. In addition, a lifetime average factor would be smaller than an initial loading factor because of preferential depletion.

Differences in power level from one module to another can occur if the fuel modules are not all axially aligned. Seed misalignment effects are due to seed assembly mechanism latching differences and to core assembly base plate misalignment. Data taken during periodic physics tests show relative seed assembly position indications which differ by a few hundredths of an inch from one another, and vary from one time to the next. The total power effect is about ± 0.1%. Base plate misalignment varies from one module to another and any effect on power would be included in the measured symmetry data presented in Table IV-8.

The power allowance factors applied to the PDQ calculated power versus time, to obtain best estimate power data for core examination rods, included: 1) factors from measured flux wire data (Table IV-8B), 2) support post factors

(Table IV-8C) and 3) the axial power peak factors between grids (Table IV-8D). The grid dip factors (Table IV-8D) may be applied to selected fuel rod segments. Radial symmetry factors (Table IV-8A) and the power effect due to seed misalignment were judged to be negligible and are not included in the best estimate power data. Also, factors for fuel loading variation, which vary from rod-to-rod, are not included.

TABLE IV-1

SUMMARY OF LWBR POWER OPERATION

Operation Parameter	Design Lifetime	Extended Lifetime	Total Lifetime
Total hours	26442	17968	44410
Depletion (EFPH)	18298	10432	28730
Average power level (%)	69.20	58.06	64.69
Depletion (MWd/t)*	9300	5300	14600
Gross electric energy (10^9KWhe)	1.35	0.75	2.10
Net electric energy (10^9KWhe)	1.11	0.59	1.70
Hours at power	19743	14107	33850
Availability factor (%)**	74.7	78.5	76.2
Capacity factor (%)***	70.2	54.9	64.0
Average power level while at power (%)	92.7	74.0	84.9

*Tonne of Th + U in active height (84 inches) of the twelve central modules.
**Availability = 100 x hours plant generated power/total hours
***Capacity factor = 100 x net MWh/(design electric rating x total hours)

TABLE IV-2

TYPICAL LWBR MEASURED REACTIVITY COEFFICIENTS

Power coefficient,* 10^{-4} $\Delta\rho/\%\ \Delta P$	-1.2
Temperature coefficient,* 10^{-4} $\Delta\rho/°F$	-2.4
Pressure coefficient,* 10^{-6} $\Delta\rho$/psi	+2.3
Equilibrium xenon worth,* 10^{-2} $\Delta\rho/100\%$ Xe	+1.66
Protactinium worth,** 10^{-2} $\Delta\rho/100\%$ Pa	+2.45

*Average of measured values between beginning-of-life and 18,298 EFPH, from References 2 and 3.
**Measured value at 10,771 EFPH, Reference 11.

TABLE IV-3

INITIAL AND END OF LIFE FISSILE LOADING DISTRIBUTION

Core Region*	Fissile Loading (kg) Beginning of life	Fissile Loading (kg) End of life	Change During Lifetime
Seed			
High Zoned	137.3	101.2	-36.1
Low Zoned	61.3	42.2	-19.1
Thoria	0.0	12.8	+12.8
Total	198.6	156.2	-42.4
Standard Blanket			
High Zoned	57.7	55.1	- 2.6
Medium Zoned	42.7	43.9	+ 1.2
Low Zoned	16.0	19.2	+ 3.2
Thoria	0.0	22.8	+22.8
Total	116.4	141.0	+24.6
Power Flattening Blanket			
High Zoned	162.3	140.2	-22.1
Medium Zoned	13.6	12.4	- 1.2
Low Zoned	10.2	10.0	- 0.2
Thoria	0.0	10.2	+10.2
Total	186.1	172.8	-13.3
Radial Reflector Blanket	0.0	37.8	+37.8
Core Total	501.1**	507.8+	+ 6.7

*High zoned, medium zoned and low zoned refer to the relative amount (w/o) of U-fissile present in various fuel rods. Descriptions of these binary fuel regions were presented in Reference 6.

**Includes 0.44 kg of U-235

+ Includes 5.7 kg of U-235. Also, it is assumed that all of the 6.0 kg of Pa-233 is allowed to decay to U-233 following core shutdown. The half-life of Pa-233 is 27 days.

TABLE IV-4

LWBR FISSILE LOADING (kg) BY MODULE TYPE

Module Regions	Module I		Module II		Module III	
	BOL†	EOL‡	BOL	EOL	BOL	EOL
Seed	16.55	12.57	16.55	12.94	16.55	13.28
Standard Blanket	16.18	19.66	9.34	11.34	6.63	8.00
Power Flattening Blanket	None	None	15.66*	14.44*	23.22*	21.62*
Total Blanket	16.18	19.66	25.00*	25.78*	29.85*	29.62*
Module Total	32.73	32.23	41.55*	38.72*	46.40*	42.90*

* Two Type II and two Type III modules have about 0.06 kg less loading due to flux well locations.
† BOL = Beginning-of-Life
‡ EOL = End-of-Life (Predicted)

TABLE IV-5

DISTRIBUTION OF POWER IN LWBR* - PERCENT OF POWER

Core Region and Fuel Types	2000 EFPH	18,300 EFPH	28,700 EFPH
3 Type I Modules			
Seed	11.52	10.80	9.90
Blanket	13.90	14.24	14.58
Total	25.42	25.04	24.48
3 Type II Modules			
Seed	9.99	9.54	8.88
Standard Blanket	7.61	7.83	8.08
Power Flattening Blanket	8.55	7.88	7.77
Total	26.15	25.25	24.73
6 Type III Modules			
Seed	17.18	17.02	16.28
Standard Blanket	10.08	10.47	10.98
Power Flattening Blanket	20.75	19.72	19.97
Total	48.01	47.21	47.23
Total Seed in 12 Modules	38.69	37.36	35.06
Total Standard Blanket	31.59	32.54	33.64
Total Power Flattening Blanket	29.30	27.60	27.74
Total Reflector Blanket	0.42	2.50	3.56
*Calculated with movable fuel positions (inches)	46	60	84

TABLE IV-6

HEAT FLUX, POWER DENSITY AND FUEL DEPLETION

Heat Flux (10^3 Btu/hr-ft^2)*	Average	Maximumt
Seed	59.5	283
Standard blanket	61.5	202
Power flattening blanket	60.2	214
Reflector blanket	5.1	75

Linear Power Density (kw/ft)*	Average	Maximumt
Seed	1.4	6.7
Standard blanket	2.7	8.9
Power flattening blanket	2.4	8.6
Reflector blanket	0.3	4.5

Fuel Depletion (10^{20} fissions/cm^3)	Average		Maximumt	
	18,300 EFPH	End-of-Life	18,300 EFPH	End-of-Life
Seed**	3.2	5.1	8.3	11.4
Standard blanket**	1.6	2.7	3.4	5.3
Power flattening blanket**	1.5	2.4	3.9	5.7
Reflector blanket	0.03	0.07	0.53	1.0

Fuel Depletin (10^3 MWd/t of Th + U)	Average		Maximumt	
	18,300 EFPH	End-of-Life	18,300 EFPH	End-of-Life
Seed**	15.5	24.3	38.9	53.4
Standard blanket**	7.4	11.8	15.2	23.2
Power flattening blanket**	6.9	11.0	17.0	25.2
Reflector blanket	0.16	0.31	2.4	4.5

---

* Heat fluxes and linear power densities are for 100 EFPH except for the reflector blanket were the values are for end-of-life. All values are normalized to 236.6 MWth.

** Average depletion based on 84 inch active core height, excluding 20 inches of ThO_2 axial reflector. Multiply by 84/104 to get depletion for total fuel.

† Maximum values include allowances discussed in Section IV.D.3 for uncertainties in the nuclear analysis model and for experiment-to-calculation biases.

TABLE IV-7

LWBR CORE POWER AND DEPLETION PEAKING FACTORS‡

Core Region	Peak Local Heat Flux* / Region Avg. Heat Flux	Peak Rod Power* / Region Power	Peak Local Fissions/cm^3† / Region Avg. Fissions/cm^3
Seed	4.8	2.0	2.2
Standard blanket	3.3	1.6	2.0
Power flattening blanket	3.6	1.8	2.4

* Near beginning-of-life
† Near end-of-life
‡ Peak values include allowances discussed in Section IV.D.3 for uncertainties in the nuclear analysis model and for experiment-to-calculation biases.

TABLE IV-8

ALLOWANCE IN POWER PERFORMANCE DATA

A. Radial Symmetry, Power in module/Avg. power in type

Module	Power Factor
I-1	0.995
I-2	1.000
I-3	1.006
II-1	0.994
II-2	1.000
II-3	1.006
III-1	0.998
III-2	1.005
III-3	0.994
III-4	0.997
III-5	1.005
III-6	1.000

B. Radial Flux Wire Data, (E/C)*/(E/C) for Type II

Module Type	Power Factor
I	1.01
II	1.0
III	0.99
IV	1.06 (Typical)**
V	1.06 (Typical)

*E/C = Ratio of experiment-to-calculation.
**Factor is 1.13 at flux well location and $\sim$ 1.0 for rods near apex (see text).

TABLE IV-8

ALLOWANCE IN POWER PERFORMANCE DATA

(Continued)

C. Rods Adjacent to Support Posts

Location	Power Factor
Seed rod row 15	1.066
Blanket rod in row 5, near post at core center	0.95
Blanket and PFB row 5, rods near other posts	0.98

D. Axial Grid Factors

Region	Between Grids	Grid dip
Seed	1.03	0.95
Standard blanket	1.03	0.96
Power flattening blanket	1.03	0.98

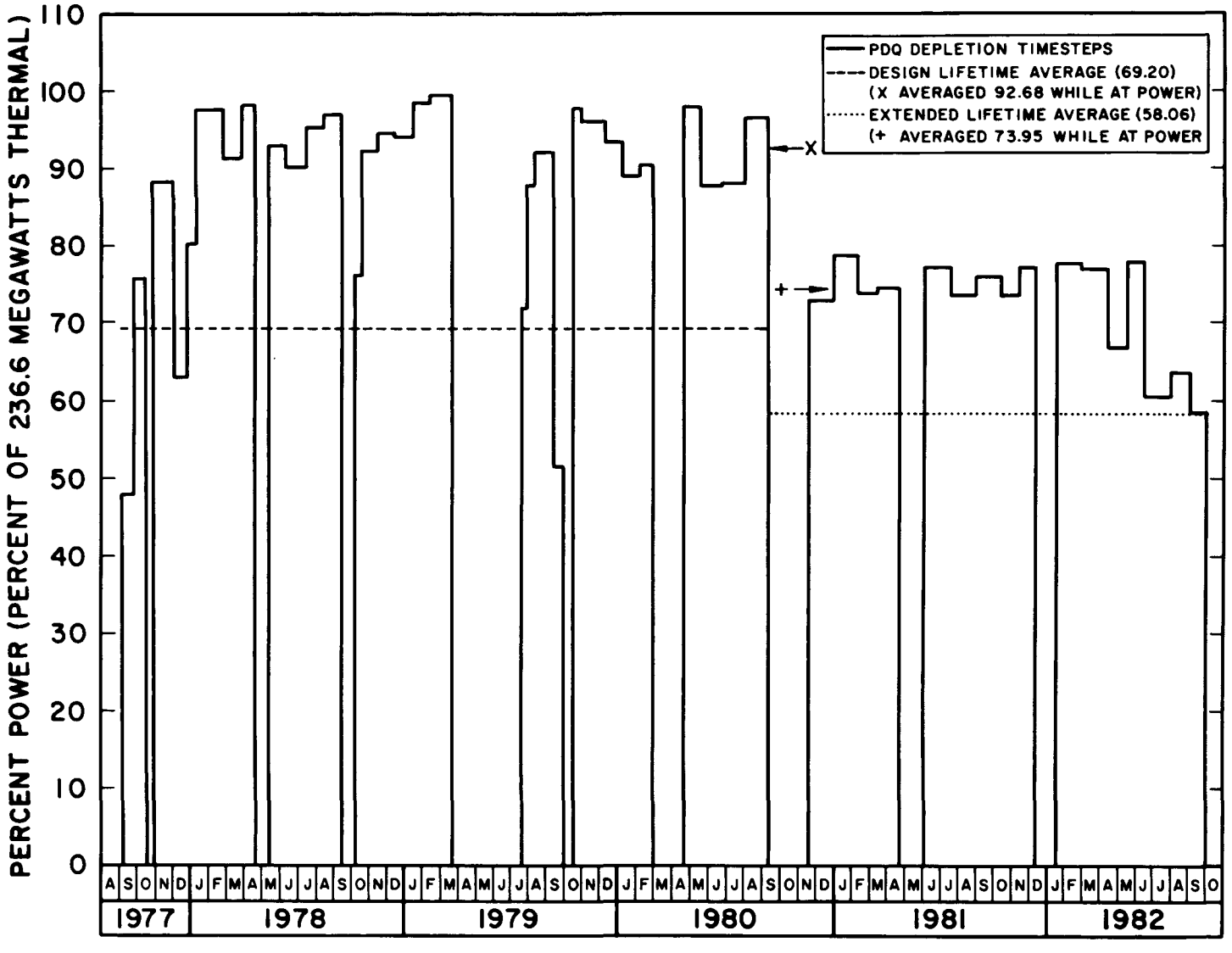

FIGURE IV-1 LWBR DEPLETION HISTORY USED IN CORE FOLLOW CALCULATIONS

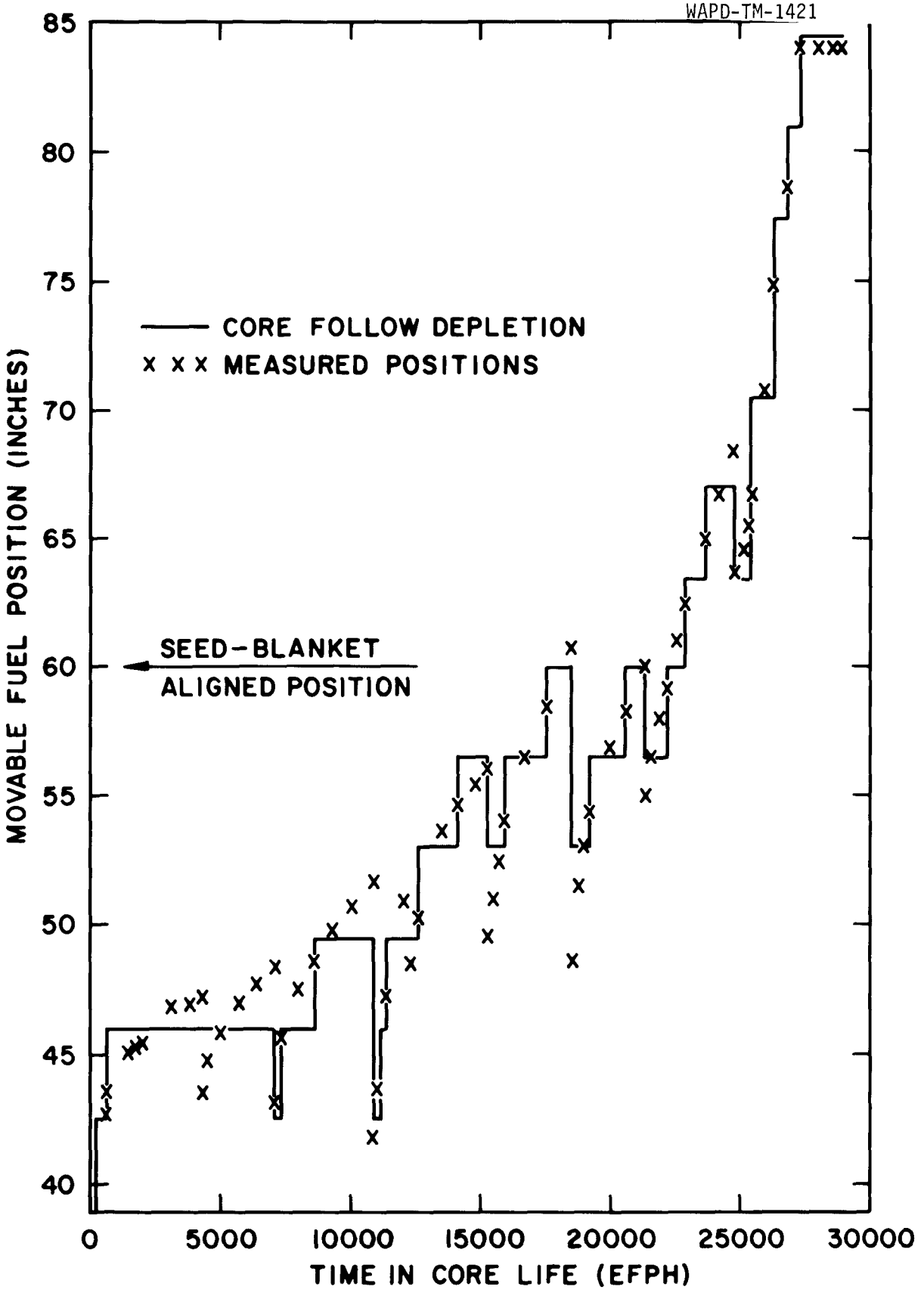

FIGURE IV-2 LWBR MOVABLE FUEL POSITIONS VERSUS TIME IN CORE LIFE AT POWER

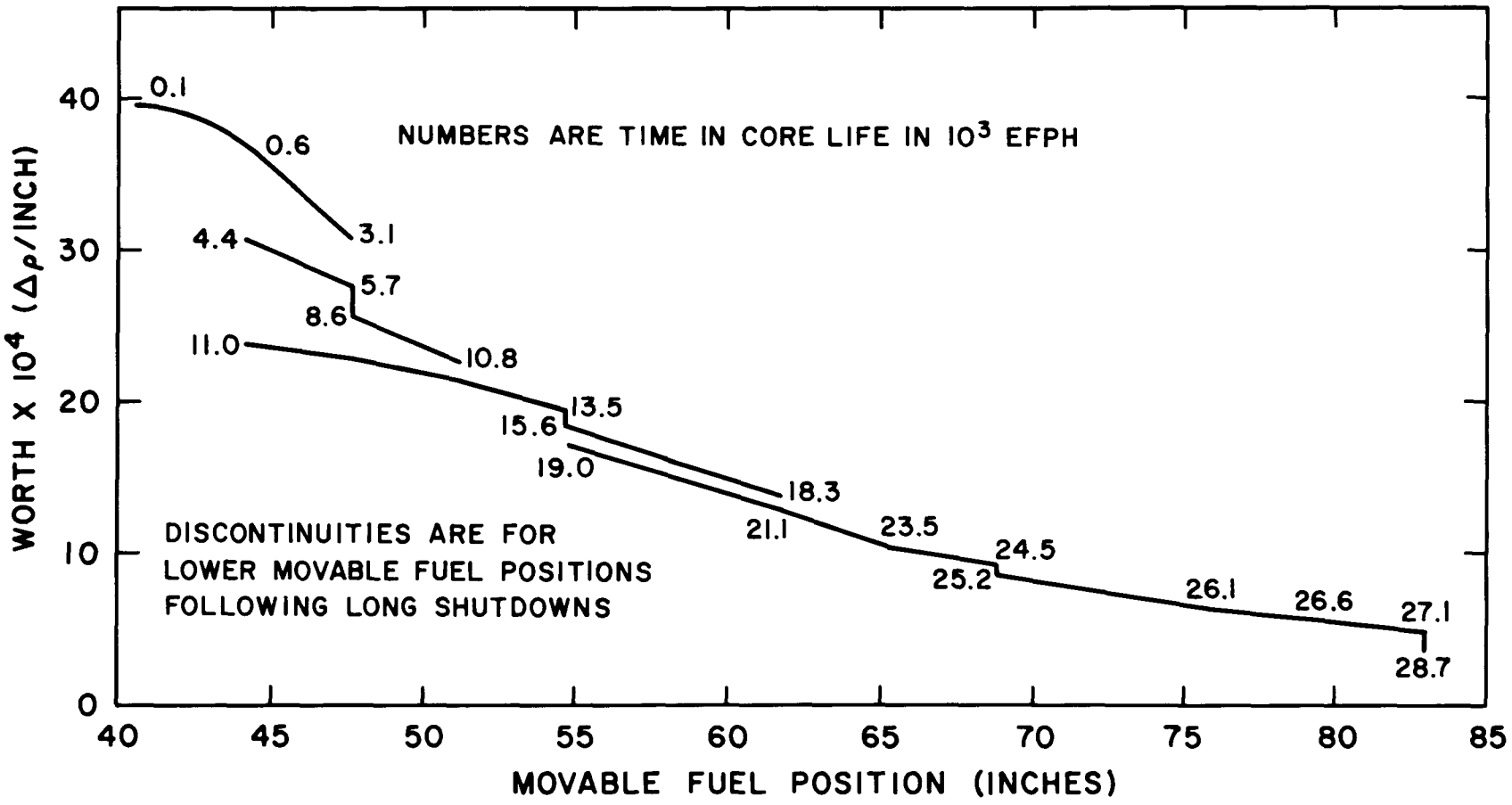

FIGURE IV-3 CALCULATED MOVABLE FUEL WORTH AT POWER VS POSITION FOR THE 12 SEED BANK

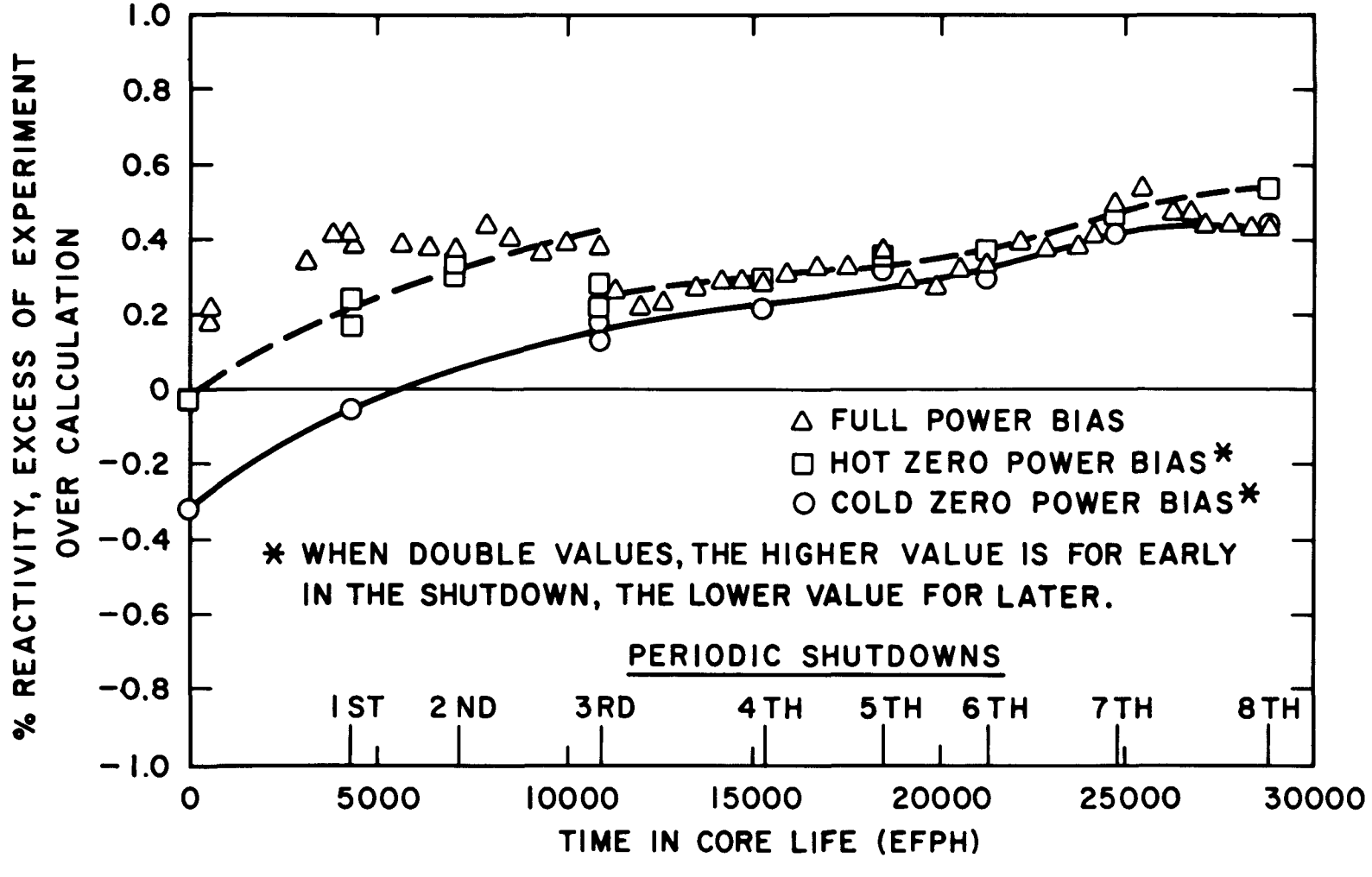

FIGURE IV-4 LWBR REACTIVITY BIAS

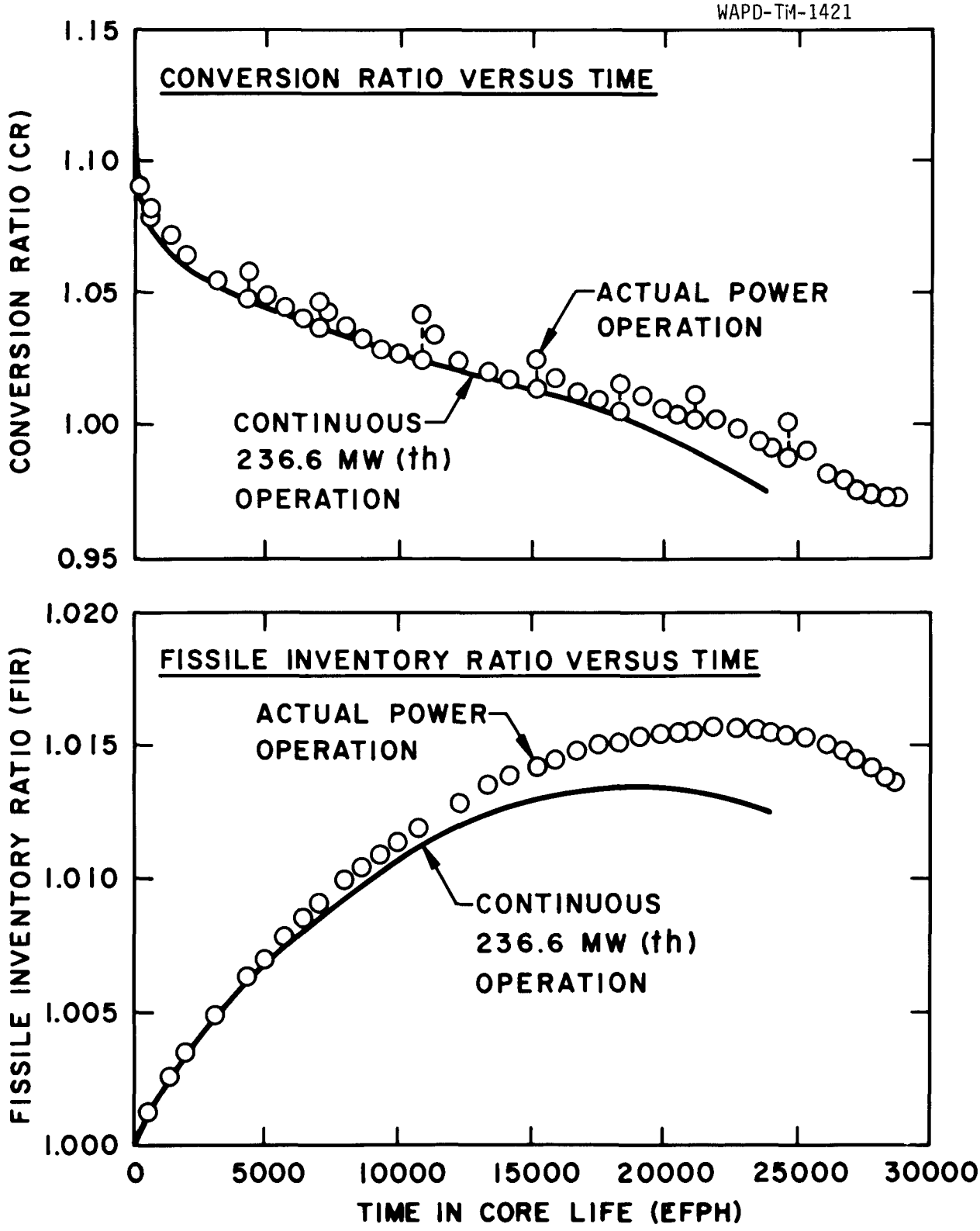

FIGURE IV-5 CALCULATED BREEDING IN LWBR

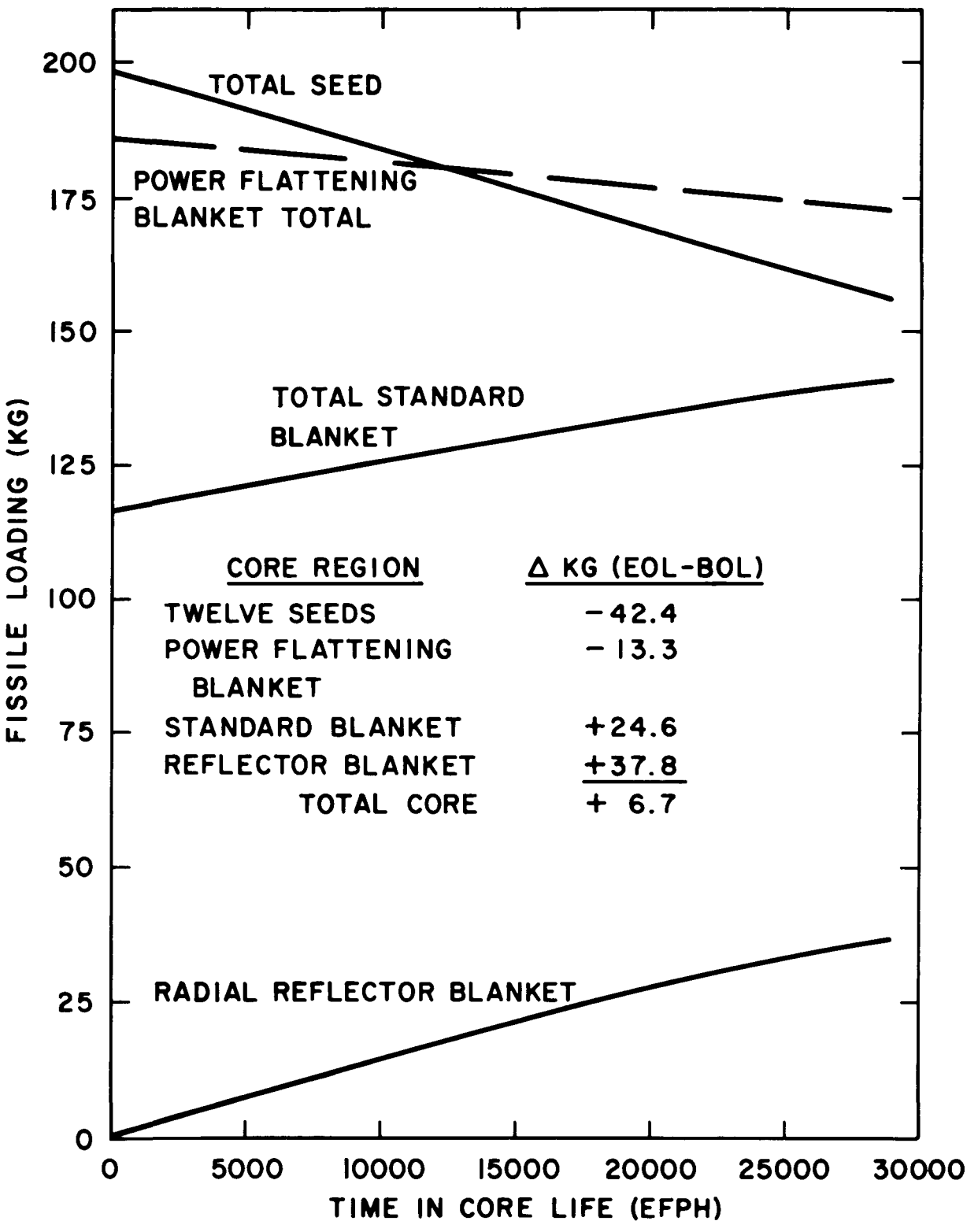

FIGURE IV-6 REGION FISSILE LOADINGS

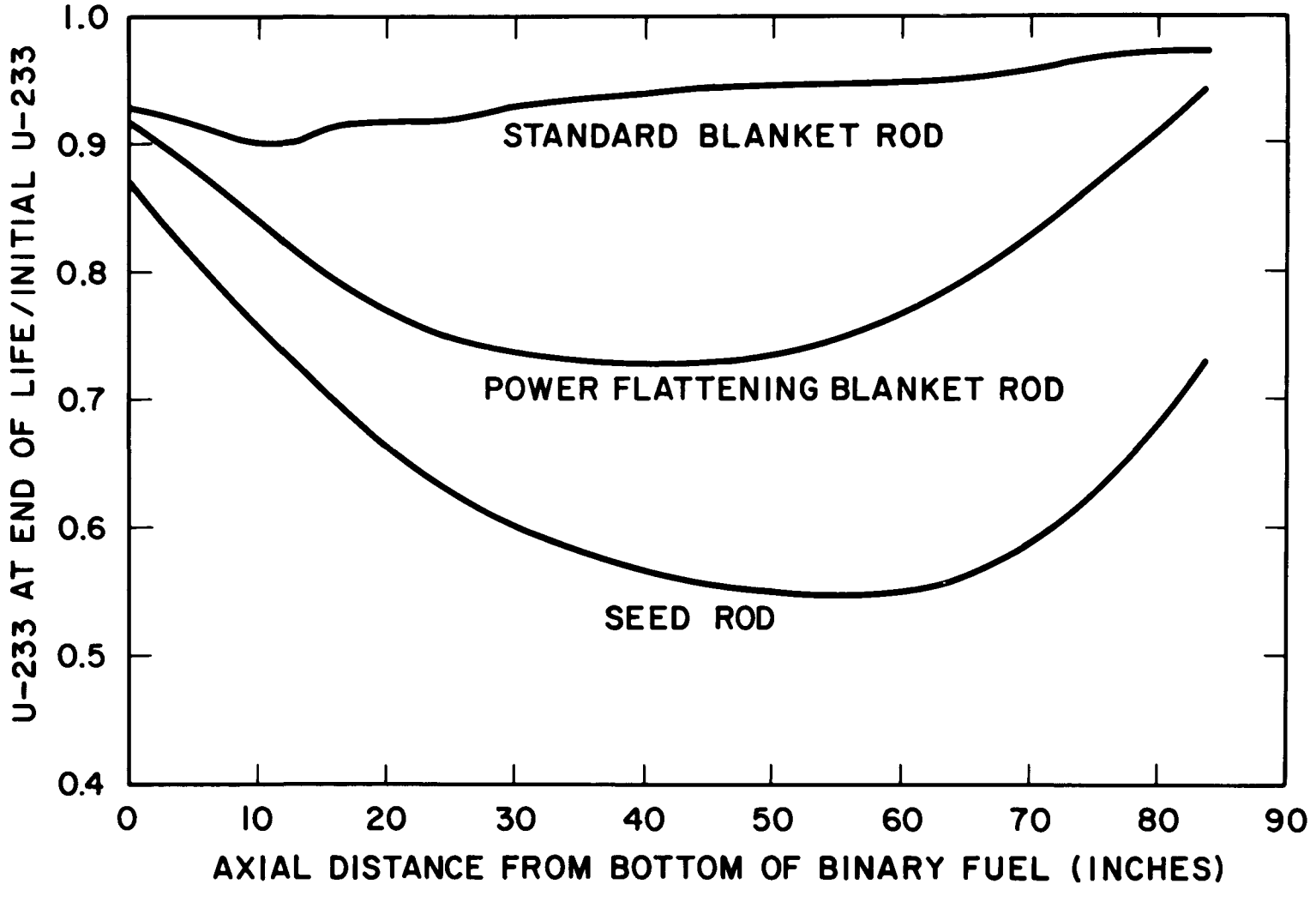

FIGURE IV-7 AXIAL U-233 DISTRIBUTION IN 84-INCH BINARY RODS

(MAXIMUM DEPLETED RODS AT END OF LIFE)

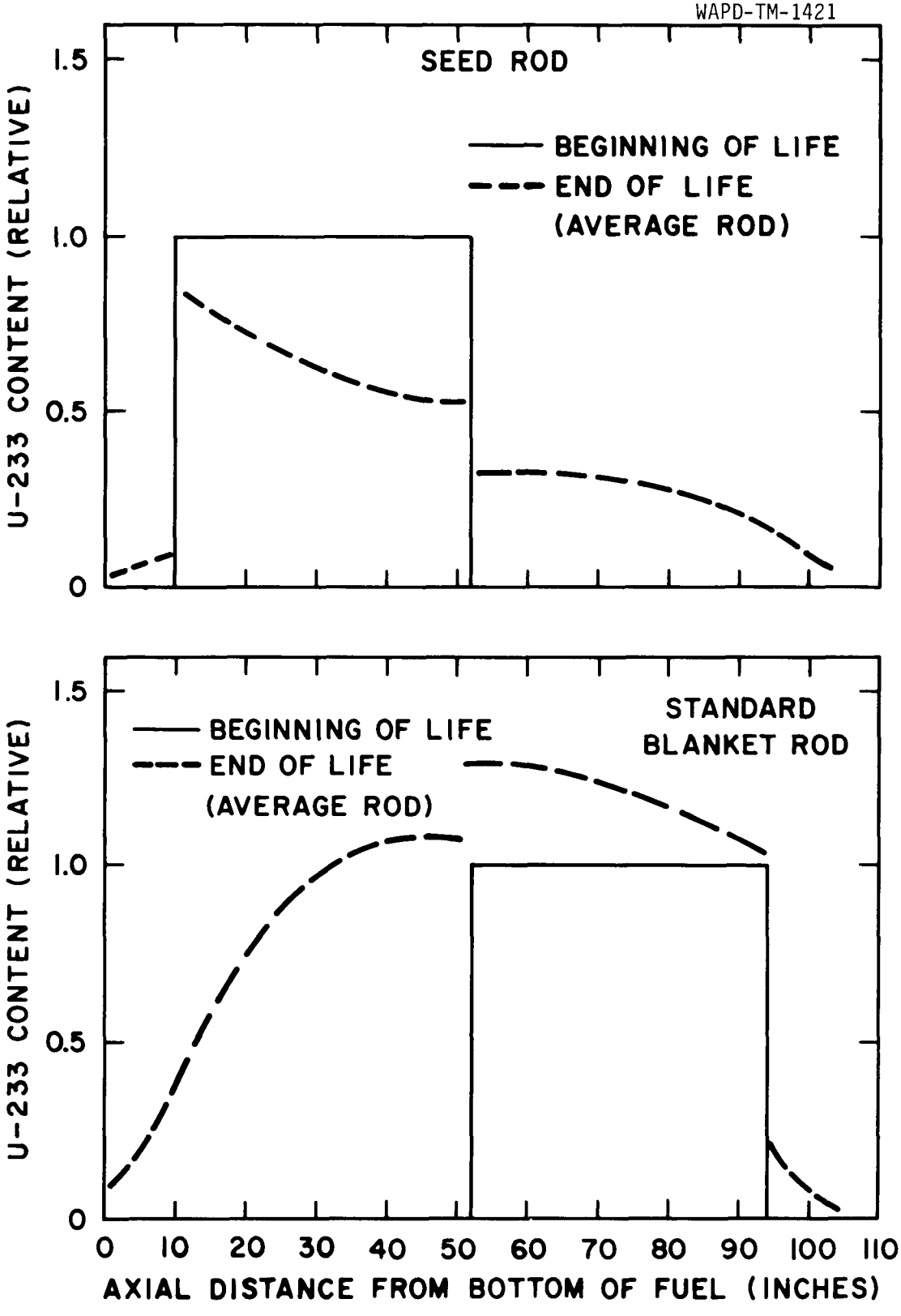

FIGURE IV-8 AXIAL U-233 DISTRIBUTION IN 42-INCH BINARY RODS

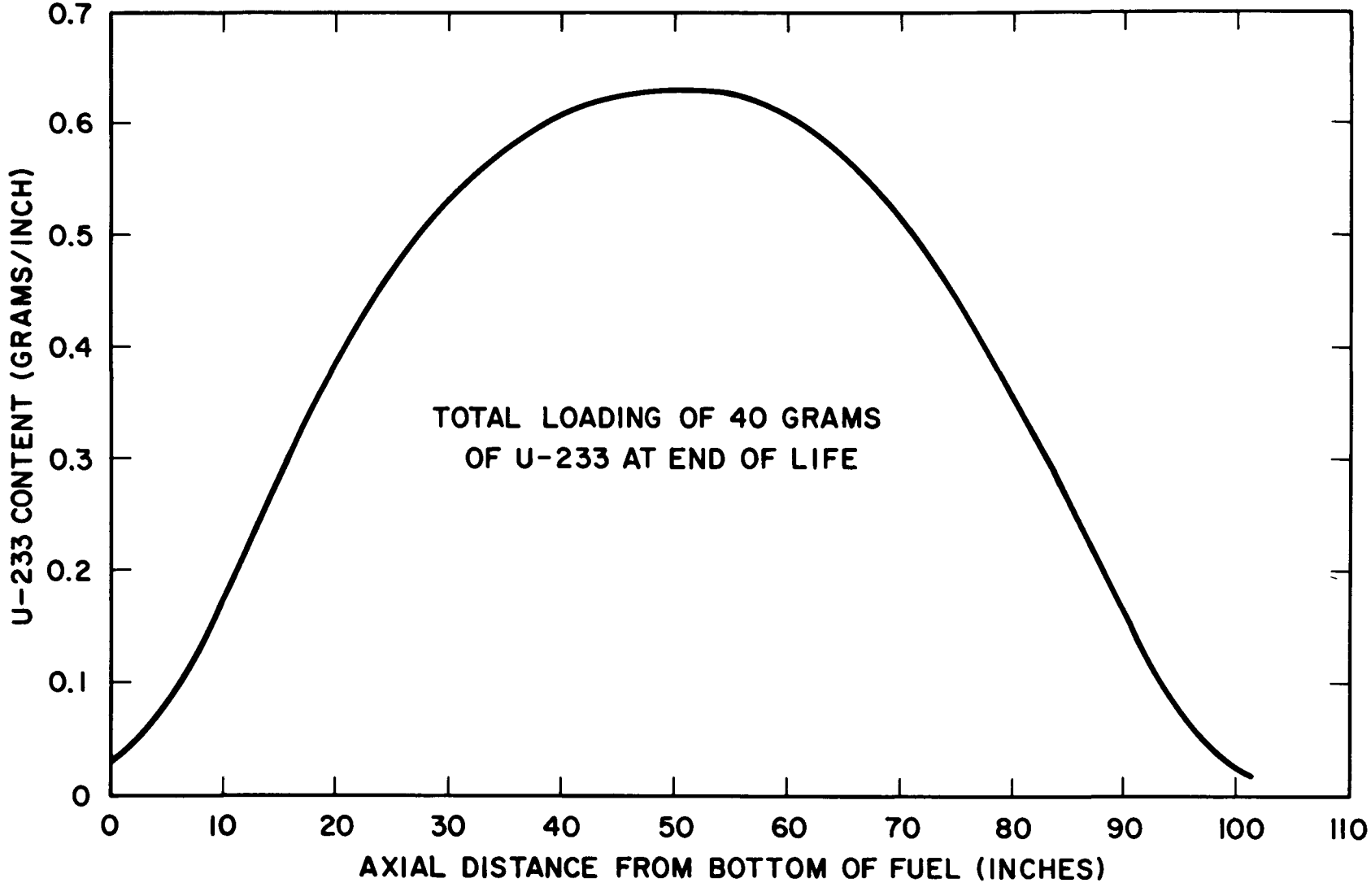

FIGURE IV-9 AXIAL U-233 DISTRIBUTION IN A REFLECTOR BLANKET ROD AT END-OF-LIFE, ROD WITH LARGEST U-233 BUILDUP

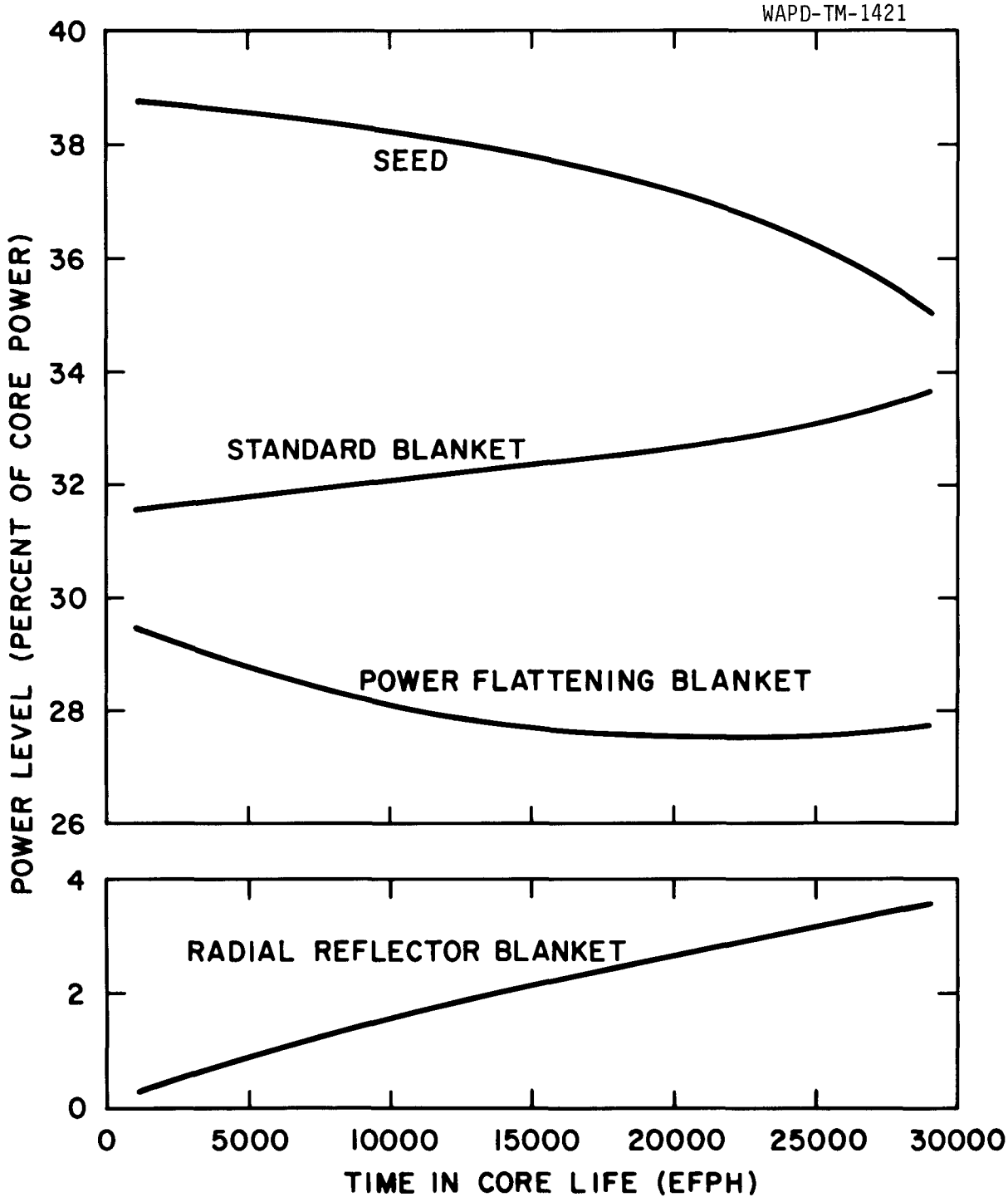

FIGURE IV-10 REGION POWER LEVELS-PERCENT OF POWER

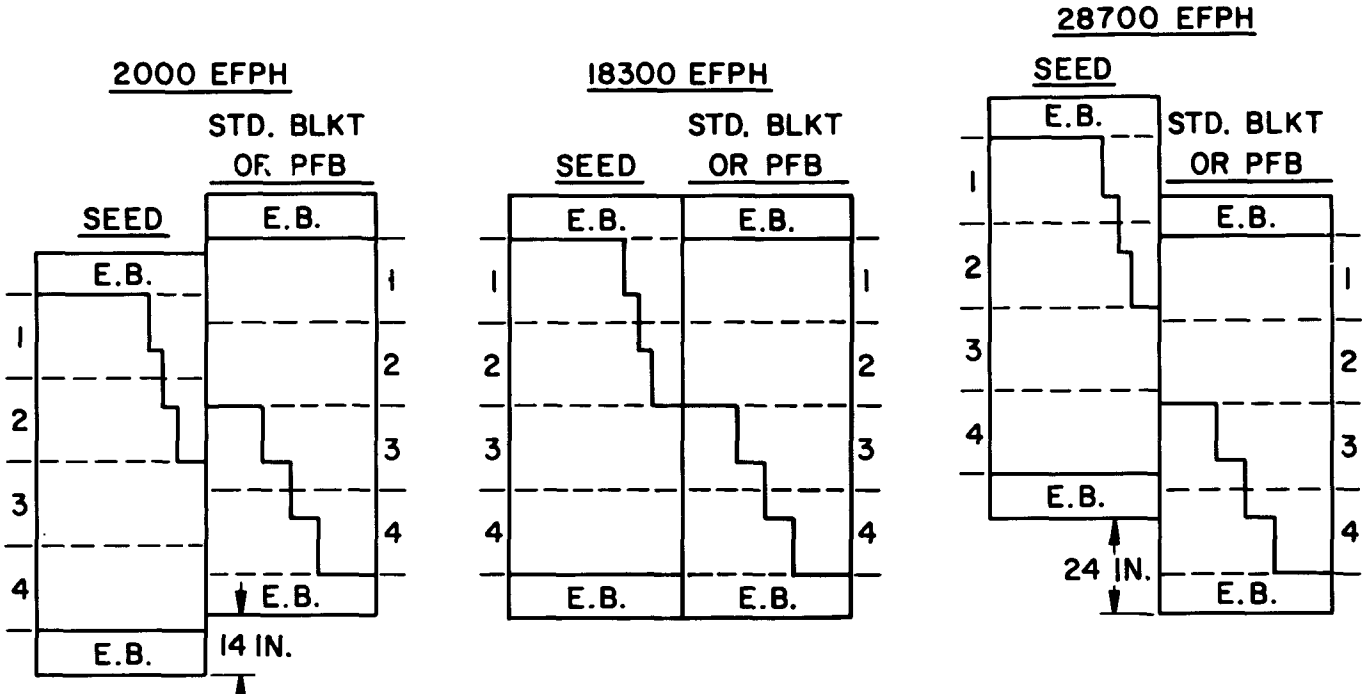

ZONE	SEED	BLKT	PFB	SEED	BLKT	PFB	SEED	BLKT	PFB
1	9.19	4.26	3.86	4.92	5.83	5.01	0.42	8.32	7.20
2	13.88	13.39	11.66	9.42	10.20	8.57	6.00	13.60	11.21
3	12.78	10.00	9.56	13.35	10.62	8.97	13.49	10.39	8.23
4	2.78	3.92	4.21	9.55	5.75	4.99	14.88	1.20	1.04
E.B.	0.06	0.02	0.01	0.12	0.14	0.06	0.27	0.13	0.06
TOTAL	38.69	31.59	29.30	37.36	32.54	27.60	35.06	33.64	27.74

PFB = POWER FLATTENING BLANKET
E.B. = ThO_2 END BLANKET

FIGURE IV-11 AXIAL POWER DISTRIBUTION IN LWBR–PERCENT OF POWER FOR NOMINAL FULL POWER, EQUILIBRIUM XENON AND PROTACTINIUM

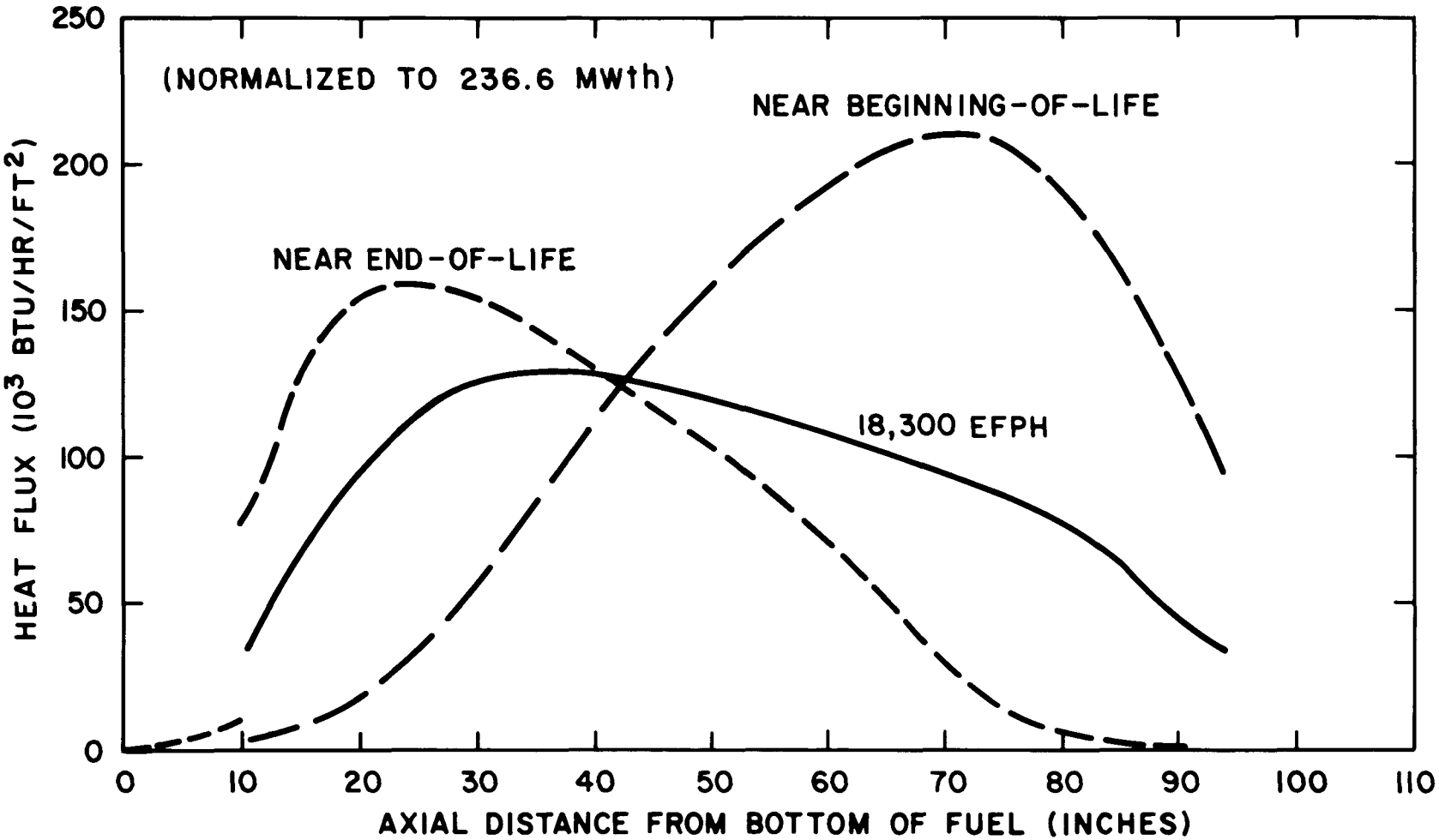

FIGURE IV-12 AXIAL POWER SHAPES IN HIGH ZONE SEED ROD

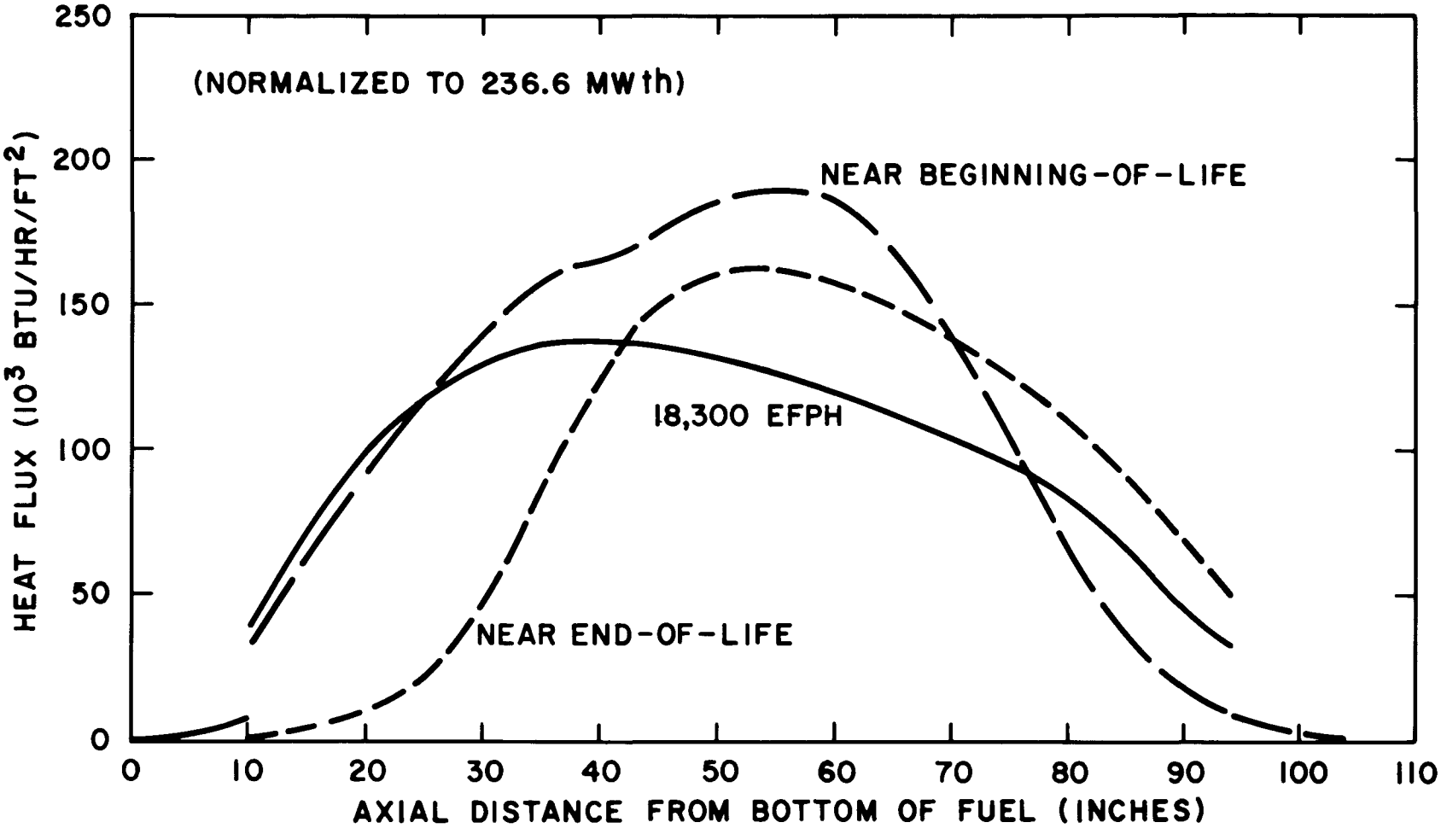

FIGURE IV-13 AXIAL POWER SHAPES IN HIGH ZONE STANDARD BLANKET ROD

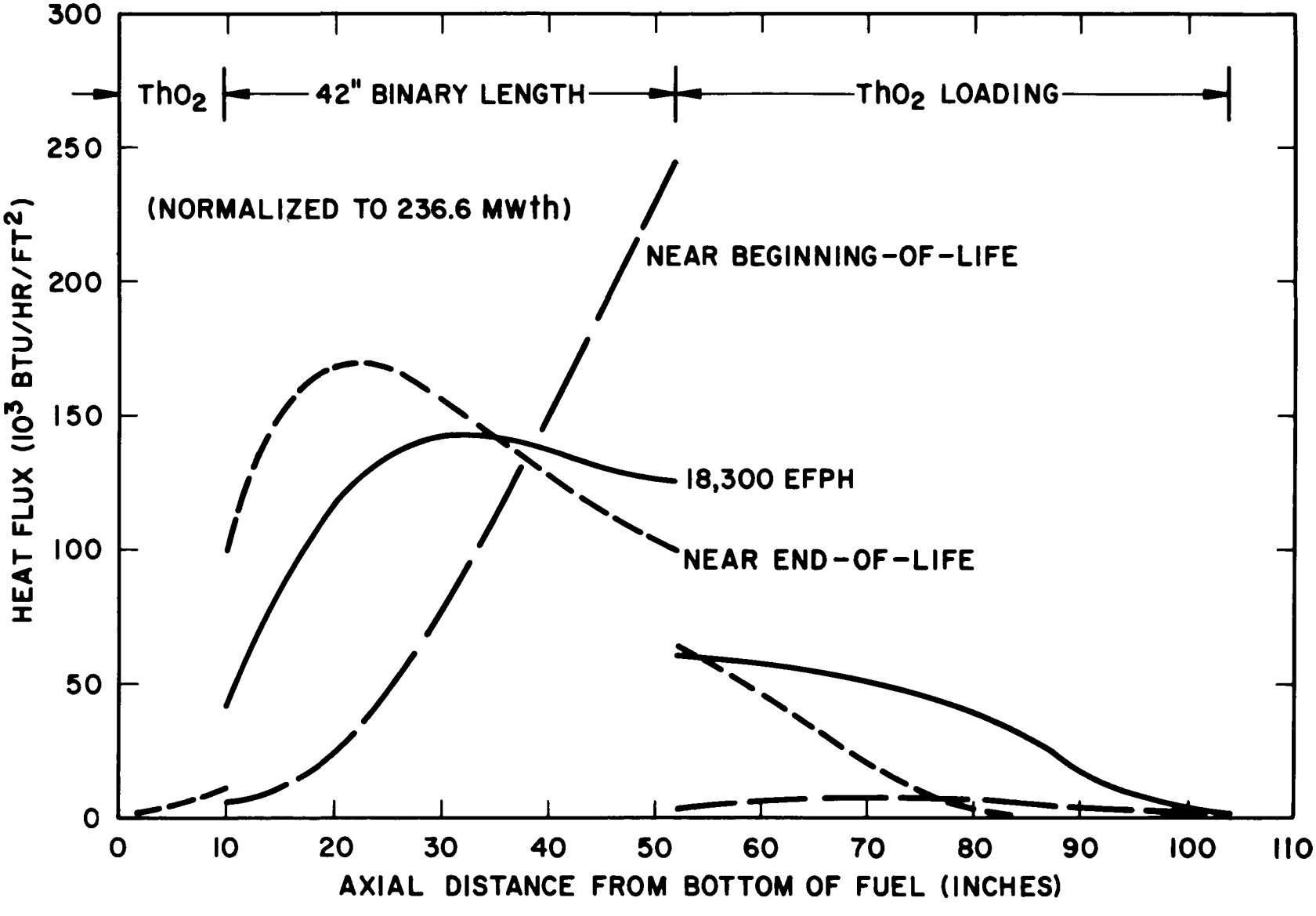

FIGURE IV-14 AXIAL POWER SHAPES IN LOW ZONE SEED ROD

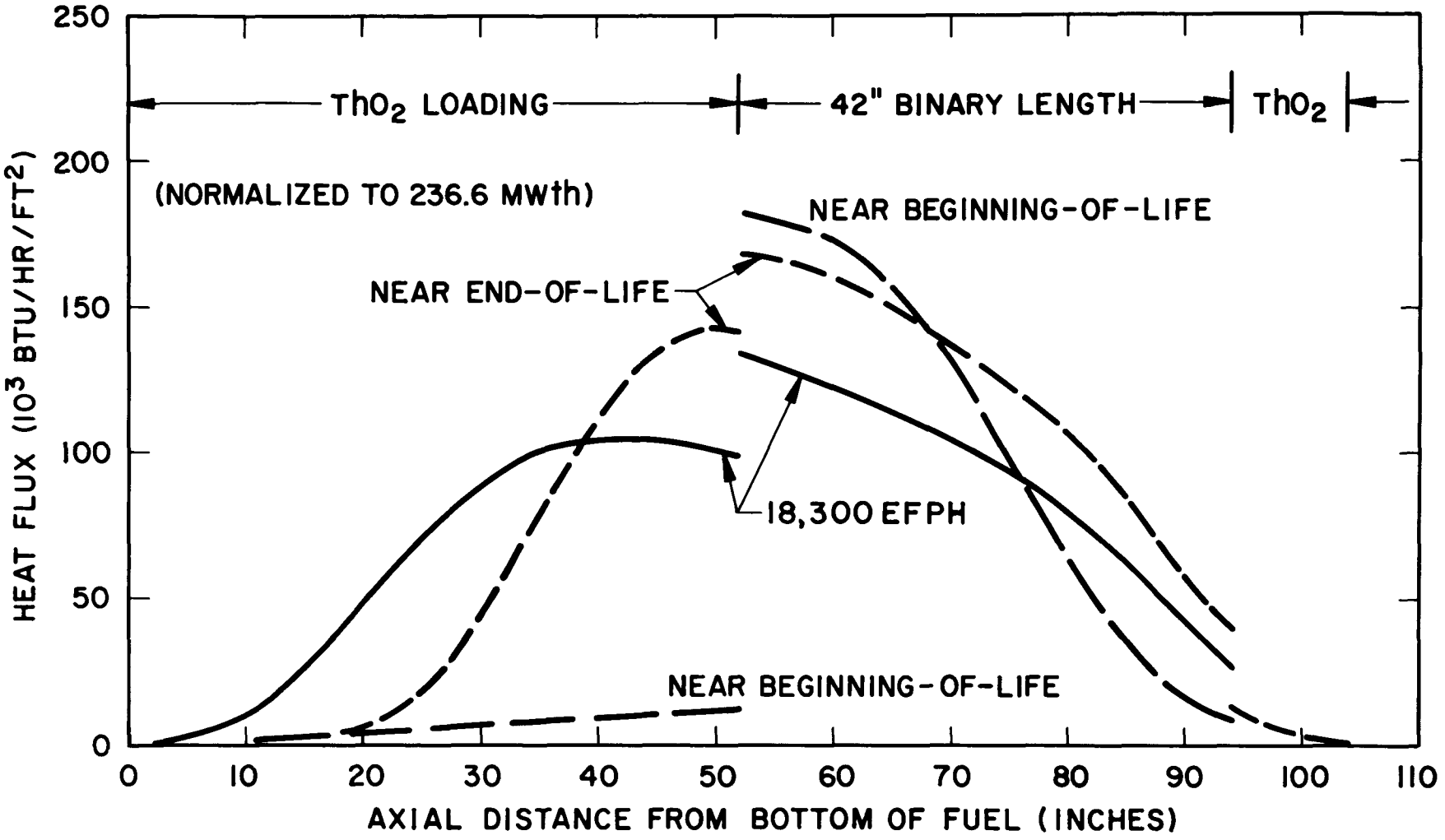

FIGURE IV-15 AXIAL POWER SHAPES IN LOW ZONE STANDARD BLANKET ROD

V. CONCLUSIONS

Operation of LWBR at Shippingport to 28,730 EFPH exceeded the design lifetime of 18,000 EFPH by 60 percent. Operation during the design lifetime included 204 planned swingloads as a demonstration of fuel element and plant capability to follow load demand for a typical utility power system. There has been no indication of fuel element failure. During the extended lifetime, maximum power level operation was at 80 percent of nominal full power (18,298 EFPH to 27,100 EFPH), to reduce the duty requirements on the fuel elements and to lengthen the reactivity lifetime of the core; a 6% further extension in lifetime was obtained by a gradual power coastdown to 57% power prior to the final shutdown at 28,730 EFPH.

The capacity factor during the design lifetime was 70.2%, and the overall capacity factor of 64 percent is above the average of commercial cores despite LWBR being the first-of-a-kind, and including all test periods and the reduced power operation. This performance attests to the care taken to design and manufacture the reactor plant, the care taken to operate the reactor plant, and also the care taken to develop accurate calculational models to predict reactor behavior.

Reactivity bias throughout core operation was well within the off-nominal allowance of $\pm 1\%\ \Delta\rho$ used in predicting the lifetime performance of LWBR. In addition, the measured test results reported in References 1, 2 and 3 confirm the adequacy of the ranges for the various nuclear design parameters assumed in the LWBR Safety Analysis Report (Reference 16).

The final fissile fuel loading of the core is calculated to be 1.3 percent greater than the initial fissile inventory built into the core. The ability of the nuclear performance analysis model to predict performance of the LWBR provides confidence in our overall capability of predicting the behavior of U^{233}-Th systems with depletion and in the estimate of breeding performance. Confirmation that LWBR did breed is expected to be shown by the proof-of-breeding program (Reference 17).

In conclusion, the LWBR core operated as predicted by the calculational model through 14,600 MWd/t of power generation and numerous testing periods, without the benefit of a full scale mockup or of any similar predecessor core. It is expected that the proof-of-breeding program will also confirm that breeding has occurred.

VI. REFERENCES.

1. W. K. Sarber, Ed., "Results of Initial Nuclear Tests in LWBR", WAPD-TM-1336, June 1979.

2. W. K. Sarber, "Reactor Physics Experimental Program for the Light Water Breeder Reactor (LWBR) at Shippingport", WAPD-TM-1455, December 1981.

3. W. K. Sarber, "Reactor Physics Experimental Program for the Light Water Breeder Reactor (LWBR) at Shippingport," WAPD-TM-1455 addendum, December 1983; see also Trans. Am. Nucl. Soc., 44, 552 and 553 (1983).

4. H. C. Hecker and L.B. Freeman," Design Features of the Light Water Breeder Reactor (LWBR) which Improve Fuel Utilization in Light Water Reactors", WAPD-TM-1409, August 1981.

5. D. R. Connors, S. Milani, J. A. Fest, and R. Atherton, "Design of the Shippingport Light Water Breeder Reactor," WAPD-TM-1208, January 1979.

6. H. C. Hecker, Jr., "Summary of the Nuclear Design and Performance of the Light Water Breeder Reactor (LWBR)," WAPD-TM-1326, June 1979; see also Trans. Am. Nucl. Soc., 28, 733 (1978) and 44, 551 (1983).

7. L. B. Freeman, Ed. "The Calculational Model Used in the Analysis of Nuclear Performance of the Light Water Breeder (LWBR)," WAPD-TM-1314, August 1978; see also Trans. Am. Nucl. Soc., 28, 731 (1978).

8. C. J. Pfeifer and C. J. Sptiz, "PDQ08 Reference Manual," WAPD-TM-1266, May 1978.

9. H. Bohl., Jr. and A. P. Hemphill, "MUFT-5, A Fast Neutron Spectrum Program for the Philco-2000," WAPD-TM-218, February 1961. Updated versions of MUFT and KATE (Reference 10) are contained in the PAX program for the CDC-6600 and 7600 computers.

10. H. J. Amster and J. B. Callaghan, "KATE-1, A Program for Calculating Wigner-Wilkens and Maxwellian Averaged Thermal Constants on the Philco-2000," WAPD-TM-232, October 1960.

11. L. B. Freeman and H. C. Hecker, "The Reactivity Worth of Protactinium-233 Inferred from Measurements," Nuclear Science and Engineering 80, 338 (1982).

12. T. R. England, W. B. Wilson, M. G. Stamatelatos, "Fission Product Data for Thermal Reactors," Los Alamos Scientific Laboratory report LA-6746-MS (EPRI-NP-356), December 1976.

13. T. R. England, "CINDER - A One-Point Depletion and Fission Product Program" WAPD-TM-334 (Revised), June 1964. Also, T. R. England, R. Wilczynski, and N. L. Whitemore, "CINDER-7: An Interim Report for Users," Los Alamos Scientific Laboratory report LA-5885-MS, April 1975.

14. W. C. Shick, Jr., S. Milani, E. Duncombe, "A Model for Incorporating Fuel Swelling and Clad Shrinkage Effects in Diffusion Theory Calculations," WAPD-TM-1369, March 1980.

15. J. B. Newman, J. F. Giovengo, and L. P. Comden, "The CYGRO-4 Fuel Rod Analysis Computer Program (LWBR/AWBA Development Program)," WAPD-TM-1300, July 1977.

16. Safety Analysis Report for the Light Water Breeder Reactor, 1975.

17. W. C. Schick, Jr., W. J. Beggs, A. C. Kahler, G. Tessler, "The LWBR Proof-of-Breeding Program," Trans. Am. Nucl. Soc., 45, 713 (1983).

18. T. R. England, G. L. Hartfield, and R. K. Deremer, "Xenon Spatial Stability in Large Seed - Blanket Reactors," WAPD-TM-606, April 1967.

19. L. B. Freeman, G. L. Hartfield, W. K. Sarber, and D. M. Rowland, "Measured Xenon Stability of a ^{233}U-Th Reactor," Trans. Am. Nucl. Soc., 35, 595 (1980).

20. J. A. Mitchell, Ed., "BMU Series U^{233} Fueled Critical Experiments," WAPD-TM-1117, January 1975.

21. G. G. Smith, J. P. Semans, J. A. Mitchell, Eds., "U^{233} Oxide-Thorium Oxide Detailed Cell Critical Experiments," WAPD-TM-1101, October 1974.

22. N. R. Candelore, R. C. Gast, L. A. Ondis II, "RCP01 - A Monte Carlo Program for Solving Neutron and Photon Transport Problems in Three-Dimensional Geometry with Detailed Energy Description," WAPD-TM-1267, August 1978.

ACKNOWLEDGEMENTS

The design and development of the LWBR core at the Bettis Atomic Power Laboratory evolved through the efforts of a large group of engineers and scientists over a period of more than a decade. The author wishes to acknowledge the efforts of B. R. Beaudoin and J. A. Milan who processed the measured core data, and R. J. Eckert who performed the core follow calculations for the first year of operation.

Technical guidance and management for the performance of the core follow calculations and the preparation of this report were provided by M. Natelson, S. Milani, L. B. Freeman and I. Goldberg.

The typing efforts of the 1-AT Word processing staff during the preparation of this report are appreciated.

*U.S. GOVERNMENT PRINTING OFFICE 1984/705-032/363